Simulating sediment supply from the Congo watershed over the last 155 ka

Stéphane Molliex, Albert Kettner, Dimitri Laurent, Laurence Droz, Tania Marsset, Alain Laraque, Marina Rabineau, Guy Moukandi N'Kaya

Simulating sediment supply from the Congo watershed over the last 155 ka

Molliex Stéphane [1, *], Kettner Albert J. [2], Laurent Dimitri [3], Droz Laurence [6], Marsset Tania [3], Laraque Alain [4], Rabineau Marina [6], N'Kaya Guy D. Moukandi [5]

[1] Univ Bretagne Occidentale, CNRS, IUEM, Lab Geosci Ocean,Labex Mer,UMR 6538, F-29280 Plouzane, France.
[2] Univ Colorado, Inst Arctic & Alpine Res, CSDMS, Dartmouth Flood Observ, Boulder, CO 80309 USA.
[3] IFREMER, UR Geosci Marines, BP 70, F-29280 Plouzane, France.
[4] OMP, F-31400 Toulouse, France.
[5] Univ Marien Ngouabi, LMEI CUSI ENSP, BP 69, Brazzaville, Rep Congo.

* Corresponding author : Stéphane Molliex, email address : smolliex@gmail.com

Abstract :

The Congo River is the world's second largest river in terms of drainage area and water discharge. Monitored for decades, a large dataset is available, onshore for both the hydrology and sediment load, and offshore by many paleo-environmental proxies compiled at the Late-Quaternary time-scale. These numerous data allow for accurate calibration of numerical modeling. In this study, we aim to numerically quantify the evolution of sediment supply leaving the tropical Congo watershed during the last 155 ka and to decipher the forcing parameters that control this sediment supply over glacial/interglacial stages. For this, a modified version of the model HydroTrend, that besides morphologic, climatic, hydrologic, lithologic, land cover and anthropogenic factors now also considers sediment deposition on the floodplain, is used. In addition, a method to quantify the impact of natural vegetation changes is developed.

Simulations match well the present-day observed data. They indicate that a significant portion of suspended sediments is trapped on the floodplain. Long-term simulations indicate that environmental changes between glacial and interglacial stages account for a 30% maximum variation of sediment supply. Climatic changes - precipitation and temperature, account for a maximum decrease in sediment supply of 20% during cold periods while conversely, induced land cover changes (loss of forest during colder and dryer stages) lead to enhanced sediment supply up to 30%. Over a longer period, the average sediment supply remained almost constant during glacial and interglacial periods, while peaks may have occurred during a warming period, just before forests had time to recover the catchment, i.e. during post-glacial periods. These moderate changes in sediment export, despite major changes in climate and vegetation cover, can be explained by the efficiency of sediment trapping of large tropical catchments that buffer fluvial fluxes towards the ocean.

Keywords : Glacial/interglacial, Sediment supply modeling, HydroTrend, Vegetation dynamics, Equatorial Africa, Congo watershed, Weathering, Hydrology

1- Introduction

Understanding factors and processes controlling sediment yield is crucial for a comprehensive baseline in global denudation rates, fluvial sedimentary archives, biochemical cycles and human impact on sediment fluxes (e.g. Meybeck, 2003; Walling, 2006; Syvitski and Milliman, 2007). Sediment yield can be expressed as a function of various factors including catchment morphology (area, relief, slope), lithology, climatic conditions, tectonics, vegetation, land use, impact of reservoirs (e.g. de Vente and Poesen, 2005; Syvitski and Milliman, 2007; Pelletier, 2012; Vanmaercke et al., 2014). However, the quantification of evolution of sediment yields over time remains a challenge because of the number of processes, the complexity, and the feedbacks of processes involved both on soil denudation and fluvial sediment transport (Picouet et al., 2001). In addition, the relative importance of forcing parameters depends on the size of the catchment and the climatic and tectonic context of its setting and is often poorly understood.

Large tropical catchments contain some of the richest ecosystems on Earth and provide a large part of nutrients to the oceans. Tropical zones have the largest land mass on Earth, a high transport capacity, high erosion rates due to biogeochemical weathering, and thus sediment loads are enhanced by the humid and warm climate (e.g. Xu, 2003; Zhu et al., 2007; Syvitski et al., 2017). Therefore large tropical catchments are playing an essential role in both terrestrial and marine ecosystems. Nevertheless, processes controlling sediment fluxes to the ocean are poorly understood and because of basin size, accurate quantification of these processes over time is often challenging to perform.

The Congo River is the world's second largest river in terms of both drainage area ($3.7.10^6 \, \text{km}^2$) and water discharge ($41,000 \, \text{m}^3 \, \text{s}^{-1}$) (Laraque et al., 2013). Its catchment can be considered as the most pristine major tropical watershed because it has for example far fewer dams in comparison with other large tropical watersheds such as the Amazon (Latrubesse et al., 2017) or Mekong Rivers (Ellis et al., 2012; Winemiller et al., 2016). However, because it is challenging to acquire *in-situ* data, the Congo basin has experienced much less scientific attention in basin hydrology and sediment supply than other large tropical catchments (Alsdorf et al., 2016). Unlike other major rivers, the contemporary Congo River has always maintained a connection with its deep-sea canyon, allowing for efficient transfer of

Total Suspended Sediment (TSS) directly to the abyssal plain (Rabouille et al., 2009; Vangriesheim et al., 2009). Moreover, Gingele et al. (1998) showed by studying smectite cristallinity that at least 95% of sediment deposited in the deep-sea fan is directly provided by the Congo River, with aeolian contribution being limited. These characteristics make a direct comparison between sediment supply exported from the catchment and the sediment volume deposited in the deep-sea fan possible.

Better understanding of the main controlling factors of sediment yields in Africa is also of interest from a societal perspective. Recent population growth and climatic changes in Africa have important impacts on land cover changes and water resources (e.g. Barnes, 1990; Bruijnzeel, 2004; Zhang et al., 2006; Reichenstein et al., 2013). Reliable information on the variability over time in sediment yield and its sensitivity to land cover or climate changes is therefore crucial for sustainable catchment management (Vanmaercke et al., 2014).

Recently, development of remote sensing tools have allowed for better understanding of the Congo's terrestrial water dynamics (Jung et al., 2010; Beighley et al., 2011; O'Loughlin et al., 2013; Lee et al., 2011; 2014; 2015). Moreover, numerical models such as HydroTrend, based on empirical equations can simulate water and sediment discharge of watersheds and have proven to be able to successfully reproduce basin hydrology over geological times with high accuracy (e.g. Syvitski and Miliman, 2007). These are thus reliable tools for quantifying the role of environmental forcing on fluvial processes, in particular since only 10 % of rivers have observational time series of sediment delivery to the ocean (Syvitski et al., 2005). Of those, few records reach more than a century, which is too short to fully comprehend and unravel processes influencing the fluvial sediment fluxes (Wilby et al., 1997).

However, modeling the Congo's catchment sediment supply towards the ocean is challenging because (i) the size of the catchment, which includes several climatic zones; (ii) the strong variability of land cover over time due to its sensitivity to climate changes, and (iii) of net depositional areas in the catchment that are not always clearly identifiable.

In this study, we simulate the water and suspended sediment discharge exported from the Congo's River basin over the last 155 ka by applying the hydrological transport model HydroTrend, of which the sediment module encompasses the empirical BQART function (Syvitski et al., 1998; Kettner and Syvitski, 2008). This quantification is based on a calibration by *in-situ* present-day data. The variability of water and sediment discharge over the last 155 ka is then modeled from this calibration by using available environmental proxies. These simulations aim to improve our understanding of the factors controlling sediment yield of the Congo catchment and help address societal challenges. In detail, we aim to better understand how the suspended sediment supply varies over one full climatic glacial/interglacial cycle with a focus on transitions. Which are the parameters controlling these variations and how do they control suspended sediment fluxes? We also validate our long-term

102   sediment flux simulations with published denudation and weathering rates, volumes of sediment
103   deposited offshore and basic weathering proxies determined from marine cores.

2- *Environmental setting*

105   The 4,700 km long Congo River drains 3.7 millions of km² of the center of equatorial Africa (Fig. 1),
106   and lies on both sides of the equator. Its heart is constituted by a vast (about 50% of the total drainage
107   area), low gradient (at some locations the slope is less than a few centimeter per kilometer) and
108   shallow perched basin (with altitudes ranging from 300 to 500 m) called "Cuvette Centrale" (Fig. 1A,
109   1B and 1C). This depression, is the surface expression of a Cenozoic basin, and is surrounded by
110   moderately elevated hills (1000 to 1500 m of elevation) to the North and South, and by a mountain
111   range to the East (the western shoulder of the East African Rift), where elevations reach up to 4100 m
112   (Fig. 1B). These reliefs mainly consist of crystalline basement (e.g. Lee et al., 2015). Terrains with
113   elevations higher than 2000 m only represent 0.4% of the drainage area. Drainage area located in the
114   southern hemisphere represents about 60% of the total drainage area, with a mean elevation of about
115   200 m higher than the elevation of the drainage area located in the northern hemisphere (Fig. 1A and
116   1B). The main tributaries of the Congo River are the Oubangui, the Sangha, the group of Batékés
117   Rivers on its right bank, and the Kasaï River on its left bank (Fig. 1). The headwaters of the Congo
118   catchment contain the world's second largest lake by volume and depth (Lake Tanganyika), which
119   holds approximately 17% of the world's fresh water volume (Coulter, 1991) and traps the majority of
120   sediments provided by the upstream part of the catchment (Sichingabula, 1999). In the Cuvette
121   Centrale, two very shallow (3 to 8 m deep) lakes (Tumba and Mai Ndombé) extend for more than
122   3000 km² and are situated on the left bank of the Congo River (Laraque et al., 1998). These lakes, as
123   well as the "Cuvette Centrale", which is almost permanently flooded, trap a large part of the
124   suspended sediment load. The Congo River delivers water and sediment to the Atlantic Ocean and is
125   directly and permanently connected to an active deep-sea fan through the 1,135 km-long deeply
126   incised submarine Congo Canyon and channels (Babonneau et al., 2002). This hydrographic network
127   remained relatively stable throughout the Quaternary despite sea-level and climatic changes
128   (Guillocheau et al., 2015; Flügel et al., 2015).

129   Currently, the Congo Basin experiences a humid tropical climate with three main climatic zones: a)
130   equatorial humid in the center of the basin on both sides of the Equator, b) tropical humid with a
131   monsoon season at higher latitudes, and c) tropical semi-arid with a dry season on the northern and
132   southern catchment boundaries (Kottek et al., 2006). The mean annual precipitation is 1,630 mm with
133   a mean temperature of about 24°C at Brazzaville (Bultot, 1972; Alsdorf et al., 2016) (Fig. 2A; Fig.
134   2B). Vast areas of the central Congo Basin do not experience a dry season, whereas the highlands
135   experience two wet and dry seasons (Boyer et al., 2006). The Congo River crosses the Equator twice
136   and, as a result, experiences always a rainy season somewhere in its basin during the year (Fig. 2A and

2D). The wet season for the southerly flowing tributaries is from April to September (e.g. the Oubangui River) and for the northerly flowing tributaries from October to May (e.g. the Kasai River). This results in a typically equatorial hydrological regime (Rodier, 1964; Martins and Probst, 1991) with limited monthly discharge fluctuations (Fig. 2E; 3A). As an example, for the Congo only two minor peak events in December and May and two minor low flow events in August and March occur (Coynel et al., 2005; Laraque et al., 2009; 2013a) (Fig. 3A). Intrinsically, the Congo River experiences probably the most regular and uniform hydrologic regime on Earth since its mean monthly discharge ratio (maxQ/minQ) is close to 2 and the extreme monthly discharges, recorded from 1902 onwards, range only from 23,000 to 75,500 $m^3 s^{-1}$ (Alsdorf et al., 2016). The inter-annual ratio is only 1.65 with annual discharges ranging from 33,300 to 55,200 $m^3 s^{-1}$ (Alsdorf et al., 2016). The height of the water table, inferred from lake levels (Crétaux et al., 2011; Becker et al., 2014) varies by 80 mm during the year and follows the same trend as the water balance (Precipitation minus Evapotranspiration) (Fig. 2E). Water specific discharge (runoff) stays however almost constant (35 ± 5 mm), highlighting a good relationship between surface and underground water that allows for buffering the monthly river discharge and explains part of the low variability of the hydrologic system.

The "Cuvette Centrale" is mainly covered by evergreen and swamp forest and surrounded by savannah vegetation (De Namur, 1990) (Fig. 2C and Fig. 2F). During the wet season, most of these forests are flooded, while during the dry season, they partially or completely dry (Laraque et al., 1998; Coynel et al., 2005). Anthropogenic disturbances such as sewage inputs, intensive agriculture, deforestation, and dams have not yet had a significant impact on the Congo River, which has therefore not developed any of the global change syndromes observed for most of the world's largest basins (Meybeck, 2003; Coynel et al., 2005). And therefore, the sediment dynamics are still mostly in a natural state.

The Congo River currently transports a total of 87 Mt yr^{-1} of matter to the ocean (Laraque et al. 2009, 2013b). Only one third is constituted by suspended sediment load (SSL) while the main part of matter exported is dissolved (Laraque et al. 2009, 2013b) (Fig. 3B). No accurate data is available for bed load. As for the water discharge, the mean monthly suspended sediment load is also uniform. The total dissolved matter is well correlated to the water discharge, conversely to the SSL (Fig. 3C; 3D). Because of the scarcity of high slope areas in the catchment (less than 0.0005 % of the drainage area has slopes higher than 45°), potential landslides triggered by earthquakes in upstream Congo are unlikely to significantly impact the total suspended sediment load of the catchment.

3- *Data and Method*

Our simulations were performed by removing part of the Congo Basin located upstream of Lake Tanganyika. The area upstream of Lake Tanganyika, that mainly drains the East-African Rift System, does not significantly contribute to the sediment flux towards the ocean as this lake traps large

171 portions of the upstream sediment supply (Sichingabula, 1999). For this study, the Congo River outlet

172 was considered at Brazzaville, about 480 km upstream the Congo's actual river mouth (Fig. 1A, 1C).

173 This in order to (i) calibrate our simulations with *in-situ* data available at the Brazzaville's gauging

174 station; and (ii) avoid the potential effect of sea-level fluctuations over glacial-interglacial stages to the

175 catchment, since the erosive regression of the Congo channel due to sea-level regressions does not

176 affect the catchment upstream Brazzaville, as shown by the location of the major knickpoint in the

177 longitudinal profile of the river just downstream Brazzaville (Fig. 1C). Our strategy was to calibrate

178 our simulations using present-day data, before simulating over two different timescales, the last 23 ka

179 and the last 155 ka, by integrating environmental changes, inferred from both marine and continental

180 proxies available for the study area. Simulations over these two different timescales aimed to test the

181 sensibility of the model resolution and also to study the the impact of different controlling factors

182 during climate transitions periods. Furthermore, we included to the classic HydroTrend model the

183 possibility to consider trapping in the alluvial plain, when the discharge exceeds bankfull. We also

184 developed a new methodology to consider vegetation cover variations that can occur between glacial

185 and interglacial periods.

186   *3.1 General principles of HydroTrend*

187 The HydroTrend model allows for daily simulation of discharge and sediment load leaving a river

188 system with high accuracy over long periods of time (Syvitski et al., 1998). The model incorporates

189 basin properties and biophysical processes to compute the hydrological balance (Kettner and Syvitski,

190 2008). For long-term simulations, HydroTrend has proven to be able to reproduce reliable fluvial

191 sediment yield if appropriate assumptions about past climate and land use are made (Syvitski and

192 Morehead, 1999; Kettner and Syvitsky, 2009). The structure and modules of HydroTrend have been

193 described in detail by Syvitski et al. (1998) and Kettner and Syvitski (2008), and will not be iterated

194 here. However, key equations to compute water discharge, sediment load, and trapping efficiency will

195 be described below.

196 Based on the classic water balance equation, fluvial water discharge (Q) is determined by basin area A

197 (km²), precipitation P (m yr^{-1}), evapotranspiration Ev (m^3 s^{-1}) and water storage as groundwater and

198 its release Sr (m^3 s^{-1}) (Eq. 1).

199 $$Q = A \sum_{i=1}^{ne}(P_i - Ev_i \pm Sr_i) \hspace{4cm} \text{(Eq. 1)}$$

200 Here *ne* is the number of simulated epochs (time periods with more or less similar or linear changing

201 environmental conditions), each including multiple years, and *i* is the daily time step. Following Eq.

202 (1), five hydrological processes are taken into consideration: rain (Q_r), snowmelt (Q_n), glacial melt

203 (Q_{ice}), evaporation (Q_{Ev}) and groundwater discharge (Q_g) (all in m^3 s^{-1}) (Eq. 2):

204 $$Q = Q_r + Q_n + Q_{ice} - Q_{Ev} \pm Q_g \hspace{4cm} \text{(Eq. 2)}$$

205 The long-term suspended sediment load $\bar{Q}s$ (kg s^{-1}) is computed by applying the semi-empirical

206 BQART equation described by Syvitski and Milliman (2007) (Eq. 3):

207 $\bar{Q}_s = \omega B \bar{Q}^{0.31} A^{0.5} \bar{R} T$ (Eq. 3)

208 The B term (non-dimensional) being estimated as:

209 $B = IL(1 - T_e)E_h$ (Eq. 4)

210 where ω is the proportionality coefficient defined to be 0.02 kg s^{-1} km^{-2} °C^{-1} (Syvitski and Milliman,

211 2007), $\bar{Q}$ and $\bar{R}$ are respectively non-dimensional water discharge at the river mouth and maximum

212 basin relief, following the procedure as $\bar{Q} = \left(\frac{Q}{Q_0}\right)$ and $\bar{R} = \left(\frac{R}{R_0}\right)$, where Q_0 is equal to 1 m^3 s^{-1}, and R_0

213 equals 1 m. T is the temperature at the basin outlet (°C). I, L, T_e, and E_h are non-dimensional

214 parameters, where I is a glacial erosion factor to represent the impact of glacial erosion processes, L is

215 the basin-averaged lithology factor to express the hardness of rock, and Te is the trapping efficiency by

216 natural and/or human reservoirs. Eh is the soil erosion factor related to human activities (Syvitski and

217 Milliman, 2007; Kettner and Syvitski, 2008) which is adapted for our case to consider vegetation

218 changes (see section 3.3.2 for more details).

219 To generate daily SSL fluxes, a stochastic model (Psi) is applied (Eq. 5; Morehead et al., 2003).

220 $\left(\frac{Q_{s_i}}{\bar{Q}_s}\right) = \psi_i \left(\frac{Q_i}{\bar{Q}}\right)^C$ i = 1 : m (Eq. 5)

221 where m is the total number of days (i) being modeled per epoch. The Psi model captures the inter-

222 and intra-annual variability of SSL leaving the river mouth following Eqs. (6) to (9) (Morehead et al.,

223 2003; Syvitski et al., 2005):

224 $E(\psi) = 1$ (Eq. 6)

225 $\sigma(\psi) = 0.763(0.99995)^{\bar{Q}}$ (Eq. 7)

226 $E(C) = 1.4 - 0.025T + 0.00013R + 0.145 \ln(\bar{Q}_s)$ (Eq. 8)

227 $\sigma(C) = 0.17 + 0.00000183\bar{Q}$ (Eq. 9)

228 E and σ denote respectively the mean and standard deviation of a random variable Ψ. The random

229 variable changes on a daily time step and has a log-normal distribution. C is a normal distributed

230 rating coefficient that varies over a time step of one year (Syvitsky et al., 2000). For these two

231 variables, the standard deviation depends on the mean discharge, with a power relation for ψ. These

232 equations imply that small rivers have a larger variance in C, while larger rivers have a smaller

233 variance. Notice that for short-term simulations (years to decades), because of the nature of

234 incorporated variability (Eq. 5 to 9), the daily mean suspended sediment load Q_{Si} might not exactly

235 match the long-term mean suspended sediment load $\bar{Q}_s$ as computed by BQART (Eq. 3). However,

236 these two parameters converge in long-term simulations (hundreds to thousands of years).

237 Because of the basin size and insignificant annual variability in discharge and sediment load of the

238 Congo watershed, $\sigma(C)$ (Eq. 9), using Morehead et al. (2003) provided a significant higher annual

239 variability compared to field observations. We recalculate the $E(C)$ parameter specifically for the

240 Congo based on 16 years of regularly monitoring of annual sediment load data (PEGI program,
241 Laraque et Orange, 1996; HYBAM, 2016). The observed annual standard deviation is 12 % while Eq.
242 9 predicts about 40 %. We thus recalibrated Eq. 9 to better reflect variations in sediment for the Congo
243 River (Eq. 10):

244 $$\sigma(C) = 0.17 + 0.00000056\bar{Q} \qquad\qquad\qquad \text{(Eq. 10)}$$

245 The trapping efficiency Te by natural reservoirs larger than 0.5 km^3, such as lakes, is calculated by
246 HydroTrend using the equation of Brune (1953) following Vörösmarty et al. (1997) when multiple
247 reservoirs are represented in a catchment:

248 $$T_e = \sum_{j=1}^{m} \left(1 - \frac{0.05}{\sqrt{\Delta\tau_j}}\right) \qquad\qquad\qquad \text{(Eq. 11)}$$

249 Here $\Delta\tau_j$ is the approximated residence time per sub-basin j and is estimated by

250 $$\Delta\tau_j = \frac{\sum_1^{n_i} V_i}{Q_j} \qquad\qquad\qquad \text{(Eq. 12)}$$

251 where V_i is the operational volume of the reservoir i, and Q_j is the discharge at the mouth of each sub-
252 basin j. Specifically to this study, we included in the model the possibility of additional trapping by
253 floodplains and wetlands. Many large catchments contain alluvial plains. When bankfull discharges
254 are exceed, sediment can be trapped within an alluvial plain. For the model, we considered that as the
255 discharge exceeds the bankfull threshold at a certain location (based on upstream area or certain
256 elevation in the drainage basin), sediment load is trapped on the floodplain (Qsi_{bk}) which is estimated
257 as:

258 $$Qs_{ibk} = (Q_i - Q_{bk}) \times C_{si} \qquad\qquad\qquad \text{(Eq. 13)}$$

259 where the accessible water is daily calculated as total discharge (Q_i) minus the bankfull threshold
260 (Q_{bk}), and C_{si} is the daily sediment concentration. When the bankfull threshold is reached, we assume
261 that 100% of suspended sediments is deposited in the floodplain.

262 *3.2 Input parameters for short-term calibration.*

263 The morphological characteristics of the catchment, including river length, drainage area, the delta
264 slope, hypsometry, latitude, location of reservoirs, are extracted from the Shuttle Radar Topography
265 Mission Digital Elevation Model (SRTM DEM) with a spatial resolution of 30 arc-sec (Farr et al.,
266 2007). For hydrological properties, the average velocity of the Congo River at its main Maluku
267 Trechot gauging station (30 km upstream Brazzaville, Fig. 1) is 1.23 m s^{-1} (Laraque et al., 1995).
268 Groundwater storage (350 ± 250 km^3), groundwater coefficient (15,000 m^3 s^{-1}) and groundwater
269 exponent (1.4) are deduced from satellite-inferred lakes level fluctuations (HydroWeb database:
270 http://www.legos.obs-mip.fr/en/soa/hydrologie/hydroweb/; Crétaux et al., 2011; Becker et al., 2014).
271 The mean saturated hydraulic conductivity, related to soil texture is chosen to be 315 mm/day,
272 corresponding to a moderate coarse sandy loam (Bear, 1972). A lithology factor of 0.5 (L) is assigned

273 using the classification scheme of Syvitski and Milliman (2007). All input parameters used are
274 summarized in Table 1.

275 Mean monthly temperatures at Brazzaville are compiled from the Worldclim database (Hijmans et al.,
276 2005). Mean monthly precipitations are compiled both from the Tropical Rainfall Monitoring Mission
277 (TRMM) (Wang et al., 2014) and from 277 *in-situ* climate stations compiled in the SIEREM database
278 (Boyer et al., 2006) (locations are provided in Fig. 2A). This compilation highlights a good correlation
279 between monthly precipitation and their standard deviation at the basin scale (R^2 = 0.9), which
280 suggests a low inter-annual variability and allows for the determination of the temporal standard
281 deviation of precipitation applied to TRMM data. For the Congo basin, present-day Equilibrium-Line
282 Altitude (ELA) of glaciers is about 4500 m (Osmaston and Harrison, 2005). Glacial erosion is thus
283 currently negligible since only an insignificant part of the Congo catchment lies above this elevation.

284   *3.3 Input parameter for long-term simulations*

285 Since the hydrographic network remained almost unchanged (Flügel et al., 2015) and tectonics are
286 stable throughout the Quaternary (Guillocheau et al., 2015), we can assume that only climate and land
287 cover significantly influence water and sediment discharge during the last 155 ka. Given the high
288 temporal resolution of the input data, the resolution of our simulations can be constrained to 200 years
289 for the 0-23 ka period and 1,000 years for the 0-155 ka simulation.

290   *3-3-1- Climate changes*

291 Past precipitation and temperature can be reconstructed using proxies from local marine cores and
292 global climatic models (Fig. 4). For precipitation, we use the δ^{18}O curve compiled from core MD03-
293 2707 (Weldeab et al., 2007) located in the Gulf of Guinea about 1000 km NW of the Congo's outlet.
294 This proxy is representative of the intensity of the West African Monsoon (Weldeab et al., 2007,
295 Caley et al., 2011). For temperature, we use interpolations of Weijers et al. (2007), who directly
296 interpolated the mean atmospheric temperature (MAT) from the Methylation index of Branched
297 Tetraethers (MBT) and the Cyclisation ratio of Branched Tetraethers (CBT) in core GeoB6518-1 for
298 the last 25 ka, located close to the Congo River outlet (Fig. 1). In addition to these data, for ages older
299 than 25 ka, we used the Sea Surface Temperature curve (SST) provided by Weldeab et al. (2007) from
300 core MD03-2707, since a correlation can be made at these latitudes between sub-surface marine and
301 aerial temperatures (Weaver et al., 2001). These data were then calibrated in terms of annual rainfall
302 and temperature by using present-day and Last Glacial Maximum (LGM) global climatic models
303 (CCSM4; Gent et al., 2011) (Fig. 4). Monthly variations are calibrated with simulations of Kutzbach et
304 al., (1998) and Jolly et al., (1998). A first order variation of ELA is interpolated from local estimations
305 at LGM of Osmaston and Harrison (2005), following the intensity of Marine Isotopic Stages (Lisiecki
306 and Raymo, 2005). Note that less than 1 % of the catchment is concerned by glacial erosion during the

307 coldest phases (Osmaston and Harrison, 2005). Therefore, glacial erosion has only a limited impact

308 during the cold stages on the fluvial sediment flux.

309   *3-3-2- Land cover changes*

310 Long-term land cover changes are constrained using recent data as well as a detailed pollen study of

311 core KZaï-02 (Dalibard et al., 2014), collected in 1998 on the Congo deep-sea fan, 248 km off the

312 Congo River mouth, during the ZaïAngo1 cruise (Savoye et al., 1998) (Fig. 1) to identify historical

313 land cover changes. In order to quantify the impact of these changes in our simulations, we used an

314 approach based both on a satellite derived land cover map (GLC-SHARE; Latham et al., 2014) and on

315 monthly   NDVI   maps   MOD13A3   provided   by   NASA

316 (https://lpdaac.usgs.gov/dataset_discovery/modis/modis_products_table/mod13a3; Huete et al., 2002)

317 (Fig. 5). NDVI (Normalized Difference Vegetation Index) (Tucker, 1979) is a widely used index in

318 remote sensing studies (e.g. Xie et al., 2008). It is based on green vegetation and varies between 0 for

319 bare soil to 1 if the soil is entirely covered, so protected by vegetation (e.g. Crippen, 1990). We

320 compiled a mean annual NDVI map for the Congo catchment by averaging 12 contiguous monthly

321 NDVI maps MOD13A3 (period 2000-2001). Annual NDVI ranges from 0.35 for the sparsest

322 grasslands and crops to 0.85 for the densest rainforests (Fig. 5C). We then computed the relationship

323 between mean annual value of NDVI ($NDVI_y$) and the proportion of forested areas for 100 x 100 km

324 tiles in the catchment *Fs* (Fig. 5D). A correlation of $R^2 = 0.52$ was found between forests and the

325 $NDVI_y$. This relationship is stronger if only forests located below 900 m of elevation are involved (R^2

326 $= 0.68$) (Fig. 5D), the correlation equation being:

327 $NDVI_Y = 0.00187 \times Fs + 0.574$ (Eq. 14)

328 Within the catchment, the elevation of 900 m corresponds to the lowest limit of mountainous type

329 forests. We also compiled an evolution curve of the percentage of non-mountainous forests in the

330 catchment using pollen data (Dalibard et al., 2014) and determined equivalent paleo-NDVI values

331 from each epoch (age step) by using the correlation equation (Eq. 14) (Fig. 4E; 4F).

332 We can then determine a soil cover factor *Cf* from these paleo-NDVI values. *Cf* = 0 if vegetation cover

333 is negligible (i.e. bare soil), and *Cf* = 1 if the vegetation entirely covers the soil. A maximum soil cover

334 factor *Cf* can be determined by using the maximum amplitude of present-day *NDVIy* values (i.e. 0.85

335 for densest rainforest and 0.35 for sparsest grasslands and crops) and assuming that $Cf_{max} = 1$ for the

336 highest NDVI value (0.85; 100 % of forests) and $Cf_{max} = 0$ for the lowest NDVI value (0.35; 0% of

337 forests) (Fig. 4F). The minimum soil cover factor can be calculated from the amplitude of NDVI

338 determined from the correlation between present-day NDVI and proportion of forest (eq. 14),

339 assuming that $Cf_{min} = 1$ for 100 % of forests (NDVI = 0.76) and $Cf_{min} = 0$ for 0 % of forest (NDVI =

340 0.57). These values can be assumed as minimum because where there is no forest nowadays,

10

341 vegetation is mainly constituted by savannah. But during colder periods, such as during the LGM,

342 non-forested vegetation was probably much sparser, with a lower NDVI value.

343 In that case, C$_{max}$ and C_{min} are thus calculated as following:

344 $Cf_{max} = (0.85 - 0.35)F + 0.35$ (Eq. 15a)

345 $Cf_{min} = (0.76 - 0.57)F + 0.57$ (Eq. 15b)

346 This parameter is integrated in the BQART equation by using the erosion factor parameter *Eh* (Eq. 4),

347 such that:

348 $E_h = (1 - Cf) \times 2$ (Eq. 16)

349 We add a factor of 2 to ensure that a normal erosion factor (Eh =1) corresponds to a moderate

350 vegetation cover, which has a *NDVI$_y$* of 0.5.

351 Ratios of erosion factors between grassland, savannah and non-mountainous forests are consistent

352 with ratios obtained from *in-sit*u measurements of soil erosion in Africa under similar environmental

353 conditions (Dunne, 1979; Lal, 1985; El-Hassanin et al., 1993).

4- Results

4.1 Model calibration with present-day in-situ data

356 We first calibrated simulated water discharge to 114 years of monthly observed data available for

357 Brazzaville/Kinshasa gauging station (1902-2016) (GRDC, 2016; HYBAM, 2016) (Fig. 6). A good

358 correlation between the ranked monthly discharges observed and simulated by HydroTrend can be

359 noticed (Fig. 6B), proving that HydroTrend is able to accurately simulate the Congo discharge at an

360 annual scale, despite the large basin size and the heterogeneous climate of the catchment. The annual-

361 averaged simulated discharge is 41,650 m^3 s^{-1} and compares well with observations (41,480 m^3 s^{-1}). At

362 a monthly scale, simulated discharges match observed data for May to October, while the model

363 underestimates by about 20% the discharges from November to January and overestimates discharges

364 by about 20 % from February to April (Fig. 6C). These uncertainties may be due to difference of

365 drainage area and/or morphology between the northern hemisphere (~ 40 % of the total drainage area,

366 600 m of mean elevation) and the southern hemisphere (~ 60 % of the total drainage area, 800 m of

367 mean elevation) parts of the catchment.

368 To calibrate SSL (Suspended Sediment Load), we used in-situ monitoring data at Brazzaville station,

369 collected through several sources: preliminary survey in the 70s (Giresse and Moguedet, published in

370 Kinga-Mouzeo, 1986), continuous once-a-month survey between 1987 and 1993 (PEGI program,

371 Laraque et Orange, 1996) and continuous once-a-month survey from 2005 to present-day (HYBAM,

372   2016). Some complementary data are also available from Spencer et al., (2016). To compare observed

373   and simulated data we simulated 20 years of daily sediment discharge. First, a simulation of SSL

374   without any trapping shows a large discordance between observed and simulated data (Fig. 7A). Then,

375   we added a classic trapping, that would most likely occurs in the low-slope lands of the Cuvette

376   Centrale, which could be interpreted similarly as trapping in a lake. Simulation shows that this kind of

377   trapping is not sufficient to match *in-situ* data, especially during high-discharge events (Fig. 7B). To

378   adjust for these high-discharge events, we considered an additional trapping, within the wetlands of

379   the floodplain. This kind of trapping concerns only sediments exported above bankfull discharges, that

380   correspond to the discharge needed to flood the alluvial plain. Calibrating to the simulations, we get

381   the best results when bankfull discharge is 33,000 m^3 s^{-1}. This is about 20% lower than bankfull

382   discharge calculated from empirical equations (Andreadis et al., 2013), and particularly low in

383   comparison with mean annual discharge because some parts of the alluvial plains are almost

384   permanently flooded. After taking this wetland trapping into account, simulated sediment load data

385   match the observed data well (Fig. 7C). The mean SSL is respectively of 1072 kg s^{-1} for simulated

386   data and 974 kg s^{-1} for in-situ data. This difference can be explained by the lack of *in-situ*

387   measurements during very high-discharge events (> 65,000 m^3 s^{-1}) that can lead to an underestimation

388   of SSL. This underestimation is common as reliable sediment concentration measurements during

389   high-discharge events are almost impossible to measure (e.g. Syvitski et al., 2003).

390   *4.2 Simulations of the last 155 ka.*

391   Fig. 8A and B show the 500-year running averages of mean annual simulated sediment and water

392   discharge leaving the Congo catchment over the last 155 ka. A change in water discharge correlated

393   with climatic periods can be observed, with a mean discharge ranging from 40,000 to 50,000 m^3 s^{-1}

394   during warm stages (MIS 1, 5a, 5c, 5e) and around 35,000 m^3 s^{-1} during main cold stages (MIS 2, 4, 6)

395   (Fig. 8). Changes in water discharge are often drastic during transitional periods. Sediment discharge

396   (Fig. 8) fluctuates more frequently. The minimum and maximum values (in grey Fig. 8) are calculated

397   with respect to assumptions about the vegetation index (see part 3.3.2). The mean SSL curve (in black

398   Fig. 8) overall indicates a negative correlation between water discharge and suspended sediment load.

399   Differences between lower (in warm periods) and higher (in cold periods) sediment discharges can

400   reach up to 50%, from 950 to 1500 kg s^{-1}. A focus on water and sediment discharges leaving the

401   Congo catchment since the last 23 ka with a higher resolution is presented in Fig. 9. It aims to improve

402   constrains on inter-annual variability and better understand the transitions between warm and cold

403   periods. As already shown for the 155 ka simulation, mean annual water discharge (in black Fig. 9A)

404   is about 25% less during the LGM. The inter-annual variation (in gray Fig. 9A) is also less during the

405   LGM (15% compared to 30% today). Mean annual SSL varies between 700 and 1900 kg s^{-1} over the

406   last 23 ka period (Fig. 9C), but the mean SSL averaged on a running mean over 100 years shows

407   variations between 950 to 1300 kg s^{-1}, with an overall average of about 1100 kg s^{-1} (in black Fig. 9D).

408   The inter-annual discharge variability is not significantly different between LGM and present-day and

409   the mean annual SSL is only about 10% higher during the LGM (in gray Fig. 9D). The highest SSL

410   corresponds to a post-glacial period (16-12 ka) and a short event around 5-6 ka (further discussed in

411   section 5.1). Two simulations, respectively without and with vegetation changes were performed (Fig.

412   9B and 9C). They aimed to highlight the importance of vegetation changes, which largely guide

413   second order variations and are responsible for the two high sediment periods previously mentioned. A

414   20 year daily simulation that considers LGM environmental conditions (21 ka) was also performed in

415   order to compare SSL between glacial and interglacial (present-day) periods (Fig. 10A). During LGM,

416   the water discharge is lower, but because of the less dense vegetation cover, the concentration of

417   sediment is higher. It results in a slightly higher SSL during LGM, and showing an increase of about

418   15% (1221 kg s^{-1} at LGM versus 1072 kg s^{-1} today). These results suggest that during cold periods, the

419   climatic conditions are theoretically less favorable to the production of sediment, notably because of

420   the lower precipitation rate. But at the same time, the regression of rainforests enhanced soil erosion

421   and thus sediment production. Therefore, the two effects have opposite consequences on sediment

422   production. Graphs of Fig. 10B and Fig. 10C aim to decipher the relative contribution of climate

423   conditions (temperature and precipitation) (red curve) and vegetation cover (green curve) with respect

424   to mean sediment load (black curve). Data are normalized for comparison with present-day. Except

425   during warm periods (MIS 1, 5c and 5e), climate factors typically cause a decrease in sediment

426   production in comparison to present-day. Decreases of forested land during colder periods enhanced

427   sediment production. This explains why the sediment load varies only by 10-15% during most of the

428   last 155 ka (except for some relatively short periods), while variations in climate conditions and

429   vegetation cover could impact up to 30% the sediment load between the more and the less favorable

430   periods (Fig. 10C). It also implies that peaks in sediment supply most likely occur when climate

431   begins to warm, after a cooling period but vegetation had no chance yet to fully recover and reconquer

432   the catchment, i.e. during post-glacial periods. In the case of the last deglaciation (16-12 ka) this peak

433   reached about 1300 kg s^{-1}, i.e. 20 % higher than what is currently observed.

434   By extrapolating the period to 155 ka, highest simulated SSL peaks occurred during the MIS 5, with

435   about 30 % more sediment than currently observed, and when climate changes were very rapid and

436   intensive, between the cold (MIS 5b and 5d) and the warm (MIS 5a, 5c, 5e) inter-stages.

437

5- *Discussion*

439   5.1 *Importance of vegetation cover changes*

440   Simulation results suggest there is a stronger control of vegetation cover on sediment load for the

441   Congo catchment over precipitation and temperatures. Vegetation cover partly protects soil from

442   eroding by intercepting raindrops, enhancing infiltration, transpiring soil water, and increasing surface
443   roughness (Rogers and Schumm, 1991; Castillo et al., 1997; Gyssels et al., 2005; Roller et al., 2012,
444   El Kateb et al., 2013). In tropical zones the vegetation cover is strongly controlled by climatic
445   conditions (Elenga et al., 2004; Dalibard et al., 2014). The sea surface temperature controls upwelling
446   and monsoon intensity (Maley et al., 1997) and directly impacts tropical rainforest development.
447   During the LGM, tropical rainforests decreased by about 70-80 % for the Congo catchment (Jolly et
448   al., 1998; Rommerkirchen et al., 2006). Simulations suggest that this decrease in rainforest could be
449   responsible for enhancing sediment production by more than 30 %, while external climatic variations
450   account only for a 20 % decrease in sediment during glacial stages. A peak of sediment load occurred
451   at around 5 ka (Fig. 9D). This sediment peak reflects a decrease in rainforest coverage during a period
452   when no change in climatic condition is detected (Fig. 10B) (Bayon et al., 2012; Dalibard et al., 2014).
453   This event, probably more accurately dated by pollen studies onshore at 3 ka (e.g. Elenga et al., 2004)
454   instead of the 5 ka that was dated by offshore proxies, was associated to a global intensification of
455   erosional processes (Maley, 1992; Bayon et al., 2012). It was interpreted as resulting from a potential
456   change in rainfall variability, due to the setting of convective atmospheric systems leading to an
457   alternation between dry periods and very strong precipitation events responsible for an increase of
458   runoff and a decrease of water infiltration (Maley, 1982; Maley et al., 2000). The presence of human
459   activities in the forest at this time, evidenced by archeological studies (Wotzka 2006; Brncic et al.
460   2007; Morin-Rivat et al., 2014) could also be a forcing factor, limiting forest development, as
461   suggested by Bayon et al. (2012), although the specific role of human impact is still largely questioned
462   (Neumann et al., 2012; Maley et al., 2012).

463   5.2 *Mass budget comparison between exported sediments, denudation and weathering rates*
464   *and sediments deposited offshore.*

465   Present-day specific sediment load exported from the Congo catchment, estimated from the most
466   recent river load compilation (Laraque et al., 2013b) is 2,725 kg s^{-1} (1,046 kg s^{-1} of TSS and 1,679 kg
467   s^{-1} of dissolved matter). This corresponds to an erosion rate of about 23 t km^{-2} yr^{-1}, consistent with the
468   19 t km^{-2} yr^{-1} indicated by previous studies (NKounkou and Probst, 1987; Summerfield and Hulton,
469   1994). Present-day global mass budget deduced from geochemical analyses is 13 t km^{-2} yr^{-1} (Gaillardet
470   et al., 1995). Different estimates are therefore of the same order of magnitude. At longer timescales
471   (10^5-10^6 years), our results suggest denudation rates of about 26 t km² yr^{-1}, considering a constant ratio
472   between suspended and dissolved sediment load. Denudation rates deduced from cosmogenic studies
473   suggest a similar rate of about 27 t km² yr^{-1} for the Congo basin (Al-Gharib, 1992), which is in the
474   same range as other cosmogenic studies for drainage basins in central and western Africa, located in
475   similar climatic, morphologic and lithologic setting. For example, 8 to 22 t km^{-2} yr^{-1} for the Burkina-
476   Faso craton (Brown et al., 1994) and 7 to 16 t km^{-2} yr^{-1} for the Nyong River in Cameroon (Regard et
477   al., 2016). These estimates are stable over long geological timescales (10^7-10^8 years), since mass

478 budgets determined from morphological studies suggest rates of 14.6 t km^{-2} yr^{-1} (Guillocheau et al.,
479 2016) to 16-22 t km^{-2} yr^{-1} over the last 35 Ma (Leturmy et al., 2003), in the same range as other but
480 similar catchments in central and western Africa (Beauvais and Chardon, 2013). This good agreement
481 between modern and long-term sediment fluxes was also evidenced in similar settings (lowland areas
482 of large catchments), such as the Amazon (Wittmann et al., 2011) but also for landscapes considered
483 in equilibrium (Clapp et al., 2001; Matmon et al., 2003; Vance et al., 2003). Offshore the Congo, most
484 of the sediments are deposited within the deep-sea fan (Droz et al., 2003; Savoye et al., 2009) since the
485 outlet of the watershed is connected to the deep canyon indifferently during high or low eustatic stages
486 (Babonneau et al., 2002). Volumes of sediment deposited in the most recent turbidite fan (axial fan)
487 were accurately estimated for several cycles of sedimentation over the last 210 ka (Picot, 2015; Picot
488 et al., 2016). The periods concerned are 0-11 ka; 11-75 ka; 75-130 ka; 130-210 ka. Decompacted
489 volumes given by Picot (2015) were transformed into mass using a density of 1.8 t m^{-3}, allowing for
490 comparison to simulated riverine sediment loads. These volumes can be compared to budgets deduced
491 from our sediment load results since more than 95 % of sediment preserved in the deep-sea fan is
492 provided by the Congo River (Gingele et al., 1998). The total decompacted volume of sediment of the
493 axial fan is about 8,500 km^3 (Picot et al., 2016) recently re-evaluated to 7,700 km^3 (Laurent et al.,
494 2017), which corresponds to an equivalent erosion rate of 18.8 ± 0.9 t km^{-2} yr^{-1} or a mean sediment
495 load of about 2200 ± 100 kg s^{-1}. These sediment loads are of the same order of magnitude as the
496 previously published erosion rates, determined using different independent methods (Al-Gharib, 1992;
497 Gaillardet et al., 1995; Leturmy et al., 2003; Guillocheau et al., 2016). This indicates that a large part
498 of exported matter, including dissolved matter, is preserved in the sediment of the deep-sea fan. Two
499 thirds of the matter exported from the Congo catchment is dissolved (Laraque et al., 2013b), but the
500 biogenic part of marine sediments represents less than 30 % of the turbidite fan sedimentation. This
501 biogenic part consists mainly of siliceous biogenic sediments (Schneider et al., 1997, Hatin et al.,
502 2017). For the Amazon, biogenic silica is formed as soon as the dissolved load comes in contact with
503 the marine domain, because of the change in redox conditions, but this biogenic silica also very
504 rapidly weathers into authigenic K-Fe-rich aluminosilicates (Michalopoulos and Aller, 2004). K-Fe-
505 rich aluminosilicates are present in the Congo sedimentary system (Giresse et al., 1988; Amouric et
506 al., 1994) suggesting that the same kind of processes may occur for the Congo dissolved matter. The
507 rapid recycling of biogenic silica to authigenic clays might explain why the biogenic part in marine
508 sediments is much lower than dissolved matter exported from the catchment.

509 In detail, decompacted volumes estimated from Laurent et al. (2017) are: 992 km^3 for the 0-11 ka
510 period, i.e. 43.9 t km^{-2} yr^{-1}; 3,730 km^3 for the 11-75 ka period, i.e. 28.4 t km^{-2} yr^{-1}; 904 km^3 for the 75-
511 130 ka period, i.e. 8 t km^{-2} yr^{-1} and 2,073 km^3 for the 130-210 ka period, i.e. 12.6 t km^{-2} yr^{-1}. The
512 period 0-75 ka presents a corresponding sediment load about three times higher than for the period 75-
513 210 ka, which is not consistent with results of the sediment load simulations. The simulations do not

514 suggest a significant difference of sediment inputs between these two periods (1,151 kg s^{-1} for 0-75 ka;
515 1,173 kg s^{-1} for 75-155 ka). A remobilization of older sediments in the most recent deposits might
516 explain this difference but the good stacking and preservation of turbidite features over the last 800 ka
517 (Droz et al., 2003; Marsset et al., 2009) argues against this assumption. Another possible explanation
518 is that very large catchments such as the Congo may buffer high-frequency oscillations (Métivier and
519 Gaudemer, 1999; Castelltort and Van den Driessche, 2003) by the more or less temporary storage of
520 sediments on the alluvial plain (Wittmann et al., 2011). Indeed, large pulses of mobile sediment may
521 be buffered if the amount of sediment stored in a floodplain is large relative to the sediment load.
522 Similar, the stream may maintain an important load of sediment when hinterland sediment production
523 is reduced, due to the presence of transportable debris stored in the floodplain (Phillips, 2003). The
524 agreement of modern and long-term output fluxes of the Congo could thus be explained by this
525 buffering capacity of the floodplain and/or of the estuary (Eisma and Kalf, 1984), while sediment
526 loads deduced from our simulations and those deduced from stratigraphic records may mismatch over
527 shorter wavelength (< 10^5 yrs) due to the same buffering effect, as demonstrated by Castelltort and
528 Van den Driessche (2003) and Simpson and Castelltort (2012) for large watersheds. In similar studies,
529 the size of the catchment has also been already evoked as a parameter allowing for the buffering of
530 water and sediment discharges over a glacial/interglacial cycle (Kettner and Syvitski, 2009). Note also
531 that only suspended sediment load is simulated here, dissolved matter and bedload might have a
532 different behavior with respect to trapping and release in the catchment and thus could also contribute
533 to explain a mismatch between sediment exportation and stratigraphic records over short wavelength.

534   *5.3 Simulation comparison with chemical proxies deduced from marine cores*

535 Numerous oceanographic cruises were conducted in the study area during the last decades (Cochonat
536 and Robin, 1992; Cochonat, 1998; Savoye, 1998; Marsset and Droz, 2010; Droz and Marsset, 2011).
537 These cruises allowed for a detailed, comprehensive offshore dataset which led to many environmental
538 studies that aimed to better understand regional paleo-environmental conditions and their implications
539 in term of source-to sink water and sediment budgets and continental weathering over a certain period
540 (e.g. Bayon et al., 2012; Dalibard et al., 2014; Picot et al., 2016; Hardy et al., 2016; Hatin et al., 2017).
541 From these studies, we retain the main classically used proxies in relation to water and sediment
542 transport capacity and intensity of weathering for comparisons with water and sediment supply
543 determined from the here presented model simulations. Note that due to the large size of the catchment
544 and its ability to buffer small wave-length variations in environmental conditions, chemical proxies
545 extracted from marine cores may only approximately represent continental conditions and should be
546 used with caution. Most of the data used were obtained from core KZaï-02 drilled during ZaïAngo1
547 cruise (Savoye et al., 1998).

548 The chemical erosion of silicates (i.e. weathering) is defined by the alteration of K-feldspar to
549 kaolinite. A high Al/K ratio reflects a high abundance of kaolinite and thus a high weathering degree
550 (e.g. Schneider et al., 1997). We thus used an Al/K semi-quantitative ratio measured with a XRF core
551 scanner for core KZaï-02 (Hatin et al., 2017). For core KZaï-01, located very close to KZaï-02 (Fig.
552 1), it was shown that quantitative measurements of Al/K (Bayon et al., 2012) follow a similar trend as
553 semi-quantitative ratios (Picot, 2015), allowing for the interpretation of semi-quantitative values as
554 representative of weathering intensity. Al/K ratio (Fig. 11C) is lower during cold periods indicating a
555 less efficient chemical weathering consistent with a lower water runoff (Fig. 11B) especially during
556 MIS2, MIS4 and MIS5b. At the same time sediment load increases (Fig. 11A) during cold stages,
557 meaning that physical erosion processes get enhanced in comparison with chemical processes. The
558 kaolinite/smectite ratio also reflects the weathering degree (Gingele et al., 1998). The
559 kaolinite/smectite ratio measured for KZaï-02 (Sionneau et al., 2010) (Fig. 11D) follows a trend
560 similar to Al/K ratio but is less clear, since this ratio responds over a large timescale and is very
561 sensitive to the sediment source (Thiry, 2000). Ti/Ca ratio is a tracer of fluvial intensity since titanium
562 is an immobile element in coarse sediment, while calcium resides in easily dissolvable minerals (e.g.
563 Adegbie et al., 2003; Govin et al., 2012). For the Congo, high values of Ti/Ca (Fig. 11E) only
564 occurred during long humid phases (MIS5e and MIS1) and thus do not systematically correlate with
565 water discharge (Fig. 11B). Short wave-length variations of water discharge are probably buffered by
566 trapping capability in the catchment (see discussion in section 5.1) and explain why the Ti/Ca ratio
567 does not accurately reflect the fluvial variation of the Congo. We also computed total organic carbon
568 (TOC) for core KZaï-02 (Picot, 2015) since it correlates well with climate cycles (Fig. 11F). We
569 observe an increase from 1% to 2-3% of TOC during cold periods. Most of this organic carbon has a
570 continental origin for recent periods (late Holocene) (Baudin et al., 2010), but the increase of TOC
571 during glacial stages is not consistent with the decrease in vegetation cover at that same period.
572 Schneider et al. (1997) deciphered continental and marine organic carbon in the Congo's marine
573 sediments over the last 200 ka and demonstrated that terrestrial organic carbon did not fluctuate
574 significantly in time, while fluctuations in TOC over glacial/interglacial stages are mainly controlled
575 by marine organic carbon. During cold periods, primary productivity might be enhanced by strong
576 trade winds which could reinforce upwelling and change thermoclines (Schneider et al., 1997; Berger
577 et al., 2002). The TOC seems thus controlled by the marine organic carbon rate, that is higher during
578 glacial stages while terrestrial conditions are less favorable for the development of vegetation and
579 exportation of organic carbon from the continent (less runoff and more sediment exported, Fig. 11B
580 and C).

581 *6- Conclusions*

582   We numerically simulated water and sediment supply exported to the ocean by the Congo, the second

583   largest river in the world in terms of discharge and drainage area, over the last 155 ka. This work is a

584   first attempt to use the numerical model HydroTrend on such a long time scale and on such a large

585   catchment. In context of the Congo, climate and land cover changes are the main drivers controlling

586   water and sediment supply to the ocean. For this study, numerous calibrating datasets existed over

587   long time scales, allowing for accurate long-term simulations ($>10^5$ years). Despite the size of the

588   watershed, HydroTrend was able to accurately simulate water discharge and sediment load exported

589   from the Congo. Climate and land cover changes were calibrated using global climate models, marine

590   proxies and remote sensing data. In particular, we developed an original approach for quantifying the

591   impact of vegetation changes. Results show that water discharge is very sensitive to climate, with a

592   decrease in discharge of about 25% during glacial stages. Sediment load is more sensitive to

593   vegetation changes than climate changes themselves. Variations in sediment load can reach up to more

594   than 30% in comparison with present-day during periods when climate began to warm and vegetation

595   did not have the chance yet to grow and extend again, i.e. during post-glacial stages. Overall, despite a

596   decrease in water discharge, the loss of rainforest enhanced soil erosion and thus sediment load

597   slightly increased during glacial stages. We also highlight that trapping is important in the catchment

598   and occurred in the wetlands and flood plains of the lowlands. This trapping act as a buffer for small

599   wave-length environmental variations, making interpretations in a source-to-sink approach more

600   challenging, from a stratigraphic, sedimentologic and chemical point of view. In future, our approach

601   and the novelties we added to HydroTrend could be applied for other large tropical catchments of e.g.

602   Africa, in order to infer the potential effect of environmental changes on water and sediment

603   discharge.

604   ## 7- *Acknowledgements*

611

612   ## *References cited*

613   Adegbie, A.T., Schneider, R.R., Röhl, U., Wefer, G., 2003. Glacial millennial-scale fluctuations in central
614   African precipitation recorded in terrigenous sediment supply and freshwater signals offshore Cameroon.
615   Palaeogeogr., Palaeoclimatol., Palaeoecol. 197(3–4), 323–333, doi:10.1016/S0031-0182(03)00474-7

616 Algharib, I., 1992. Apport des isotopes à vie moyenne de l'Uranium et du Thorium, 210Pb et 10Be dans l'étude
617   de l'érosion chimique et physique de deux grands bassins: Amazone et Congo. PhD thesis, Univ. Nice-
618   Sophia Antipolis.

619 Alsdorf, D., Beighley, E., Laraque, A., Lee, H., Tshimanga, R., O'Loughlin, F., Mahé, G., Dinga, B., Moukandi
620   G., Spencer, R.G.M., 2016. Opportunities for hydrologic research in the Congo Basin. Reviews of
621   Geophysics 54, doi:10.1002/2016RG000517.

622 Amouric, M., Parron, M., Casalini, C., Giresse, P., 1995. A (1: 1) 7-Å Fe phase and its transformation in recent
623   sediments: An HRTEM and AEM study. Clays and Clay Min. 43, 446–454.

624 Andreadis, K.A., Schumann, G. J.-P., Pavelsky, T., 2013. A simple global river bankfull width and depth
625   database. Water Resour. Res. 49, 7164–7168, doi:10.1002/wrcr.20440.

626 Babonneau, N., Savoye, B., Cremer, M., Klein, B., 2002. Morphology and architecture of the present canyon and
627   channel system of the Zaire deep-sea fan. Mar. Pet. Geol. 19, 445–467. doi:10.1016/S0264-
628   8172(02)00009-0

629 Barnes, R.F.W., 1990. Deforestation trends in tropical Africa. African Journal of Ecology 28, 161-173.

630 Baudin, F., Disnar, J.-R., Martinez, P., Dennielou, B., 2010. Distribution of the organic matter in the channel-
631   levees systems of mud-rich deep-sea fan (West Africa). Implication for deep offshore source rocks and
632   global carbon cycle. Marine and Petroleum Geology 27, 995-1010.

633 Bayon, G., Dennielou, B., Etoubleau, J., Ponzevera, E., Toucanne, S., Bermell, S., 2012a. Intensifying
634   Weathering and Land Use in Iron Age Central Africa. Science 335, 1219–1222.
635   doi:10.1126/science.1215400

636 Bear, J. 1972. Dynamics of fluids in porous media. Courier corporation, 764 pp.

637 Beauvais, A., Chardon, D., 2013. Modes, tempo, and spatial variability of Cenozoic cartonic denudation : The
638   West Afracan example. Geochemistry, Geophysics, Geosystems 14, doi:10.1002/ggge.20093

639 Becker, M., Santos da Silva, J., Calmant, S., Robinet, V., Linguet, L., Seyler, F., 2014. Water Level Fluctuations
640   in the Congo Basin Derived from ENVISAT Satellite Altimetry. Remote Sensing 6, 9340-9358.
641   doi:10.3390/rs6109340

642 Beighley, R.E., Ray, R.L., He, Y., Lee, H., Schaller, L., Andreadis, K.M., Durand, M., Alsdorf, D.E., Shum,
643   C.K., 2011. Comparing satellite derived precipitation datasets using the Hillslope River Routing (HRR)
644   model in the Congo River Basin. Hydrological Processes 25, 3216–3229. doi:10.1002/hyp.8045.

645 Berger, W.H., Lange, C.B., Wefer, G., 2002. Upwelling history of the Benguela-Namibia system: a synthesis of
646   Leg 175 results. In Wefer, G., Berger, W.H., Richter, C. (Eds.), Proc. ODP, Sci. Results 175, 1–103.

647 Boyer, J.-F., Dieulin, C., Rouche, N., Cres, A., Servat, E., Paturel, J.-E., Mahé, G., 2006. SIEREM an
648   environmental information system for water resources. 5th World FRIEND Conference, La Havana -
649   Cuba, November 2006 in Climate Variability and Change – Hydrological Impacts IAHS Publ. 308, 9-25.

650 Brncic, T.M., Willis, M.K.J., Harris, D.J., Washington, R., 2007. Culture or climate? The relative influences of
651   past processes on the composition of the lowland Congo rainforest. Philosophical Transactions of the
652   Royal Society of London B 362(1478), 229–242.

653 Brown, E.T., Bourlès, D.L., Colin, F., Sanfo, Z., Raisbeck, G.M., Yiou, Y., 1994. The development of iron crust
654   lateritic system in Burkina Faso, West Africa, examined with in-situ produced cosmogenic nuclides.
655   Earth Planet. Sci. Lett. 124, 19 – 33.

656 Bruijnzeel, L.A., 2004. Hydrological functions of tropical forests: not seeing the soil for the trees? Agriculture,
657   Ecosystems and Environment 104, 185-228.

658 Brune, G.M., 1953. Trap efficiency of reservoirs. Trans Am Geophys Union 34, 407–418.

659 Bultot, F., 1972. Atlas Climatique du Bassin Congolais. Publications de L'Institut National pour L'Etude
660   Agronomique du Congo (I.N.E.A.C.), 3° Partie, Température et Humidité de L'Air, Rosee, Température
661   du Sol.

662 Caley, T., Malaizé, B., Revel, M., Ducassou, E., Wainer, K., Ibrahim, M., Shoeaib, D., Migeon, S., Marieu, V.,
663   2011. Orbital timing of the Indian, East Asian and African boreal monsoons and the concept of a "global
664   monsoon." Quat. Sci. Rev. 30, 3705–3715. doi:10.1016/j.quascirev.2011.09.015

665 Castelltort, S., Van Den Driessche, J., 2003. How plausible are high-frequency sediment supply-driven cycles in
666   the stratigraphic record? Sedimentary Geology 157, 3–13, doi:10.1016/S0037-0738(03)00066-6.

667   Castillo, V.M., Martinez-Mena, M., Albaladejo, J., 1997. Runoff and soil loss response to vegetation removal in
668   a semiarid environment. Soil Sci. Soc. Am. J. 61, 1116 – 1121,
669   doi:10.2136/sssaj1997.03615995006100040018x.

670   Clapp, E.M., Bierman, P.R, Nichols, K.K., Pavich, M., Caffee, M., 2001. Rates of sediment supply to arroyos
671   from upland erosion determined using in situ produced cosmogenic [10]Be and [26]Al. Quaternary Research
672   55, 235–245.

673   Cochonat, P., 1998. ZAIANGO2 cruise, L'Atalante R/V. doi:10.17600/98010110

674   Cochonat, P., Robin, A., 1992. GUINESS I cruise, L'Atalante R/V. doi:10.17600/92004211

675   Coulter, G.W., 1991. Lake Tanganyika and its life. Oxford Univ. Press, New York.

676   Coynel, A., Seyler, P., Etcheber, H., Meybeck, M., Orange, D., 2005. Spatial and seasonal dynamics of total
677   suspended sediment and organic carbon species in the Congo River. Global biogeochemical cycles 19,
678   GB4019.

679   Crétaux, J.-F., Jelinski, W., Calmant, S., Kouraev, A., Vuglinski, V., Bergé-Nguyen, M., Gennero, M.-C., Nino,
680   F., Abarca Del Rio, R., Cazenave, A., Maisongrande, P., 2011. SOLS: A lake database to monitor in the
681   Near Real Time water level and storage variations from remote sensing data. Advance in Space Research
682   47, 1497-1507.

683   Crippen, R.E., 1990. Calculating the vegetation index faster, Remote Sensing of Environment 34, 71-73.

684   De Namur, C., 1990. Aperçu sur la végétation de l'Afrique Centrale Atlantique. in Lanfranchi R., Schwartz, D.
685   (eds). Paysages Quaternaires de l'Afrique Centrale Atlantique, Inst. Fr. de Rech. Sci. pour le Dev. en
686   Coop. (ORSTOM), Paris.

687   De Vente, J., Poesen, J., 2005. Predicting soil erosion and sediment yield at the basin scale: scale issues and
688   semi-quantitative models. Earth-Science Reviews 71, 95-125.

689   Dalibard, M., Popescu, S.-M., Maley, J., Baudin, F., Melinte-Dobrinescu, M.-C., Pittet, B., Marsset, T.,
690   Dennielou, B., Droz, L., Suc, J.-P., 2014. High-resolution vegetation history of West Africa during the
691   last 145 ka. Geobios 47, 183–198. doi:10.1016/j.geobios.2014.06.002

692   Droz, L., Marsset, T., 2011. REPREZAI_LEG2 cruise, Le Suroît R/V,. doi:10.17600/11020020

693   Droz, L., Marsset, T., Ondréas, H., Lopez, M., Savoye, B., Spy-Anderson, F.-L., 2003. Architecture of an active
694   mud-rich turbidite system: The Zaire Fan (Congo–Angola margin southeast Atlantic). Results from
695   ZaïAngo 1 and 2 cruises. AAPG Bull. 87, 1145–1168. doi:10.1306/03070300013

696   Dunne, T., 1979. Sediment yield and land use in tropical catchments. Journal of Hydrology 42, 281-300.

697   Elenga,H., Maley, J., Vincens, A., Farrera, I., 2004. Palaeoenvironments, Palaeoclimates and Landscape
698   development in Atlantic equatorial Afraica: a review of key sites covering the last 25 kyrs. In Battarbee
699   R.W. et al. (eds), Past Climate Variability through Europe and Africa. Kluwer Academic Publishers,
700   Dordrecht, The Netherlands, 181-198.

701   El-Hassanin, A.S., Labib, T.M., Gaber, E.I., 1993. Effect of vegetation cover and land slope on runoff and soil
702   losses from the watersheds of Burundi. Agriculture, Ecosystems and Environment 43, 301-308.

703   El Kateb, H., Zhang, H., Zhang, P., Mosandl, R., 2013. Soil erosion and surface runoff on different vegetation
704   covers and slope gradients: a field experiment in Southern Shaanxi Province, China. Catena 105, 1-10.

705   Ellis, E.E., Keil, R.G., Ingalls, A.E., Richey, J.E., Alin, S.R., 2012. Seasonal variability in the sources of
706   particulate organic matter of the Mekong River as discerned by elemental and lignin analyses. J.
707   Geophys. Res. 117, G01038, doi:10.1029/2011JG00.

708   Farr, T.G., Rosen, P.A., Caro, E., Crippen, R., Duren, R., Hensley, S., Kobrick, M., Paller, M., Rodriguez, E.,
709   Roth, L., Seal, D., Shaffer, S., Shimada, J., Umland, J., Werner, M., Oskin, M., Burbank, D.W., Alsdorf,
710   D., 2007. The Shuttle radar topography mission. Reviews of Geophysics 45, RG2004.

711   Flügel, T.J., Eckardt, F.D., Cotterill, F.P.D., 2015. The present day drainage patterns of the Congo river system
712   and their Neogene evolution. in: M.J. de Wit et al. (eds.), Geology and Resource Potential of the Congo
713   Basin, Regional Geology Reviews, Springer-Verlag Berlin Heidelberg. DOI 10.1007/978-3-642-29482-
714   2_15

715   Gaillardet, J., Dupré, B., Allègre, C.J., 1995. A global chemical budget applied to the Congo basin rivers:
716   Erosion rates and continental crust composition, Geochim. Cosmochim. Acta 59, 3469 – 3485.

717   Gent, P.R., Danabasoglu, G., Donner, L.J., Holland, M.M., Hunke, E.C., Jayne, S.R., Lawrence, D.M., Neale,
718   I.B., Rasch, P.J., Vertenstein, M., Worley, P.H., Yang, Z.-L., Zhang, M., 2011. The Community Climate
719   System Model Version 4. Journal of Climate 24, 4973-4991.

20

720   Gingele, F.X., Müller, P.M., Schneider, R.R., 1998. Orbital forcing of freshwater input in the Zaire Fan area -
721   clay mineral evidence from the last 200 kyr. Palaeogeogr. Palaeoclimatol. Palaeoecol. 138, 17–26.
722   doi:10.1016/S0031-0182(97)00121-1
723   Giresse, P., Wiewiora, A., Lacka, B., 1988. Mineral phases and processes within green peloids from two recent
724   deposits near the Congo River mouth. Clay Minerals 23, 447–458.
725   GRDC, Global Runoff Data Center, 2016. http://www.bafg.de/GRDC/EN/Home/homepage_node.html (last
726   accessed October 2016).
727   Govin, A., Holzwarth, U., Heslop, D., Ford Keeling, L., Zabel, M., Mulitza, S., Collins, J.A., Chiessi, C.M.,
728   2012. Distribution of major elements in Atlantic surface sediments (36°N–49°S): Imprint of terrigenous
729   input and continental weathering. Geochem. Geophys. Geosystems 13, Q01013.
730   doi:10.1029/2011GC003785
731   Guillocheau, F., Chelalou, R., Linol, B., Dauteuil, O., Robin, C., Mvondo, F., Callec, Y., Colin, J.-P., 2015.
732   Cenozoic Landscape Evolution in and Around the Congo Basin: Constraints from Sediments and
733   Planation Surfaces. in: M.J. de Wit et al. (eds.), Geology and Resource Potential of the Congo Basin,
734   Regional Geology Reviews, Springer-Verlag Berlin Heidelberg. DOI 10.1007/978-3-642-29482-2_14
735   Guillocheau, F., Galmier, V., Robin, C., 2016. Source to Sink study of the Congo system since 40 Myr: a
736   measurement ratio between mechanical and chemical erosion. *In* "Source to Sink: a long term perspective
737   of sediment budgets and sources characterization" meeting, Nov 2016, Rennes, France. Abstracts book,
738   p.62.
739   Gyssels, G., Poesen, J., Bochet, E., Li, Y., 2005. Impact of plant roots on the resistance of soils to erosion by
740   water: a review, Prog. Phys. Geogr., 29(2), 189 – 217.
741   Hardy, W., Penaud, A., Marret, F., Bayon, G., Marsset, T., Droz, L., 2016. Dinocyst assemblage constraints on
742   oceanographic and atmospheric processes in the eastern equatorial Atlantic over the last 44 kyr.
743   Biogeosciences 13, 4823–4841. http://dx.doi.org/10.5194/bg-13-4823-2016.
744   Hatin, T., Crosta, X., Le Hérissé, A., Droz, L., Marsset, T., 2017. Diatom response to oceanographic and climatic
745   changes in the Congo fan area, equatorial Atlantic Ocean, during the last 190 ka BP. Palaeogeogr.,
746   Palaeoclimato., Palaeoecol. 469, 47-59.
747   Hijmans, R.J., Cameron, S.E., Parra, J.L., Jones, P.G., Jarvis, A., 2005. Very high resolution interpolated climate
748   surfaces for global land areas. International Journal of Climatology 25, 1965–1978.
749   Huete, A., Disan, K., Miura, T., Rodriguez, E.P., Gao, X., Ferreira, L.G., 2002. Overview of the radiometric and
750   biophysical performance of the MODIS vegetation indices. Remote Sensing of Environment 83, 195-213.
751   HYBAM, 2016. Contrôles géodynamique, hydrologique et biogéochimique de l'érosion/altération et des
752   transferts de matière dans les bassins de l'Amazone, de l'Orénoque et du Congo. Available at
753   http://www.ore-hybam.org, (last accessed Nov. 2016).
754   Jolly, D., Harrison, S.P., Damnati, B., Bonnefille, R., 1998. Simulated climate and biomes of Africa during the
755   Qauternary: comparison with pollen and Lake Status data. Quaternary Science Reviews 17, 629-657.
756   Jung, H.K., Hamski, J., Durand, M., Alsdorf, D., Hossain, F., Lee, H., Azad Hossain, A.K.M., Hasan, K., Saleh
757   A., Khan, Zeaul Hoque, A.K.M., 2010. Characterization of complex fluvial systems using remote sensing
758   of spatial and temporal water level variations in the Amazon, Congo, and Brahmaputra Rivers, Earth
759   Surface Processes and Landforms 35, 294 –304, doi:10.1002/esp.1914.
760   Kettner, A.J., Syvitski, J.P.M., 2008. HydroTrend v. 3.0: A climate-driven hydrological transport model that
761   simulates discharge and sediment load leaving a river system. Computers & Geosciences 34 (10), 1170-
762   1183.
763   Kettner, A.J., Syvitski, J.P.M., 2009. Fluvial responses to environmental perturbations in the Northern
764   Mediterranean since the Last Glacial Maximum. Quaternary Science Reviews 28 (23), 2386-2397.
765   Kinga-Mouzeo, 1986. Transport particulaire actuel du fleuve Congo et de quelques affluents; enregistrement
766   quaternaire dans l'éventail détritique profond (sédimentologie, minéralogie et géochimie). PhD thesis,
767   Université de Perpignan. 251 pp.
768   Kottek, M., Grieser, J., Beck, C., Rudolf, B., Rubel, F., 2006. World Map of the Köppen-Geiger climate
769   classification updated. Meteorologische Zeitschrift 15(3), 259-263.
770   Kutzbach, J., Gallimore, R., Harrison, S., Behling, P., Selin, R., Laarif, F., 1998. Climate and Biome simulations
771   for the past 21,000 years. Quaternary Science Reviews 17, 473-506.

772   Lal, R., 1985. Soil erosion and sediment transport research in tropical Africa. Hydrological Sciences Journal 30
773   (2), 239-256. DOI: 10.1080/02626668509490987

774   Laraque, A., Bricquet, J.P., Berthelot, M., Olivry, J.C., 1995. Aspects hydrologiques du fleuve Congo.
775   Proceeding of PEGI international meeting 22-44 may 1993, CNRS-INSU-ORSTOM, Paris.

776   Laraque, A., Orange, D., 1996. Banque de données hydrochimiques des eaux de surfaces d'Afrique Centrale
777   (Congo et Oubangui) de 1987 à 1994. Programme PEGI-GBF, ORSTOM, Montpellier. 145 pp.

778   Laraque, A., Pouyaud, B., Rocchia, R., Robin R., Chaffaut I., Moutsambote, J.-M., Maziezoula, B., Censier, C.,
779   Albouy, Y., Elenga, H., Etcheber, H., Delaune, M., Sondag, F., Gasse, F., 1998. Origin and function of a
780   closed depression in equatorial humid zones: the lake Tele in north Congo. Journal of Hydrology 207,
781   236–253.

782   Laraque, A., Bricquet, J.P., Pandi, A., Olivry, J.C., 2009. A review of material transport by the Congo river and
783   its tributaries. Hydrological Processes 23, 3216-3224.

784   Laraque, **A.,** Bellanger, M., Adele, G., Guebanda, S., Gulemvuga, G., Pandi, A., Paturel, J.E., Robert, A., Tathy,
785   J.P., Yambele A.. 2013a. Evolutions récentes des débits du Congo, de l'Oubangui et de la Sangha. 2013a.
786   Geo-Eco-Trop. 37(1), 93-100.

787   Laraque, A., Castellanos, B., Steiger, J., Lòpez, J.L., Pandi, A., Rodriguez, M., Rosales, J., Adèle, G., Perez, J.,
788   Lagane, C., 2013b. A comparison of the suspended and dissolved matter dynamics of two large inter-
789   tropical rivers draining into the Atlantic Ocean: the Congo and the Orinoco. Hydrol. Process. 27, 2153–
790   2170. doi:10.1002/hyp.9776

791   Latham, J., Cumani, R., Rosati, I., Bloise, M., 2014. Global Land Cover SHARE (GLC-SHARE) database Beta-
792   Release Version 1.0. Rome: FAO. Accessed March 27.
793   http://www.glcn.org/downs/prj/glcshare/GLC_SHARE_beta_v1.0_2014.pdf

794   Latrubesse, E.M., Arima, E.Y., Dunne, T., Park, E., Baker, V.R., d'Horta, F.M., Wight, C., Wittmann, F.,
795   Zuanon, J., Baker, P.A., Ribas, C.C., Norgaard, R.B., Filizola, N., Ansar, A., Flyvbjerg B., and Stevaux
796   J.C., 2017. Damming the rivers of the Amazon basin. Nature 546, 363–369 doi:10.1038/nature22333

797   Laurent D., Picot M., Marsset T., Droz L., Rabineau M., Granjeon D., Molliex S., 2017. 3D stratigraphic
798   modeling of the Congo turbidite system since 210 ka: an investigation of factors controlling
799   sedimentation. EGU General Assembly, 23-28 April 2017, Vienna, Austria, Vol. 19, 08963.

800   Lee, H., Beighley, R.E., Alsdorf, D., Jung, H.-C., Shum, C.K., Duan, J., Guo, J., Yamazaki, D., Andreadis, K.,
801   2011. Characterization of terrestrial water dynamics in the Congo Basin using GRACE and satellite radar
802   altimetry, Remote Sens. Environ. 115, 3530–3538, doi:10.1016/j.rse.2011.08.015.

803   Lee, H., Jung, H.C., Yuan, T., Beighley, R.E., Duan, J., 2014. Controls of terrestrial water storage changes over
804   the central Congo Basin determined by integrating PALSAR ScanSAR, Envisat altimetry, and GRACE
805   data, in Remote Sensing of the Terrestrial Water Cycle, AGU Geophys. Monogr. 206, edited by V.
806   Lakshmi et al., pp. 117–129, John Wiley, Hoboken, N.J., doi:10.1002/9781118872086.

807   Lee, H., Yuan, T., Jung, H.C., Beighley, E., 2015. Mapping wetland water depths over the central Congo Basin
808   using PALSAR ScanSAR, Envisat altimetry, and MODIS VCF data, Remote Sens. Environ. 159, 70–79.

809   Leturmy, P., Lucazeau, F., Brigaud, F., 2003. Dynamic interactions between the Gulf of Guinea passive margin
810   and the Congo River drainage basin: 1. Morphology and mass balance. J. Geophys. Res. 108(B8), 2383,
811   doi:10.1029/2002JB001927.

812   Leopold, L.B., Maddock, T., 1953. The Hydraulic Geometry of Stream Channels and Some Physiographic
813   Implications. U.S. Geological Survey Professional Paper 252.

814   Lisiecki, L.E., Raymo, M.E., 2005. A Pliocene-Pleistocene stack of 57 globally distributed benthic $\delta 18O$
815   records. Paleoceanography 20, PA1003. doi:10.1029/2004PA001071

816   Maley, J., 1982. Dust, clouds, rain types and climatic variations in tropical North Africa. Quat. Res. 18, 1-16.

817   Maley, J., 1992. Mise en évidence d'une péjoration climatique entre ca. 2 500 et 2000 ans BP en Afrique
818   tropicale humide. Bull. Soc. Géol. France 163, 363-365.

819   Maley, J., Brenac, P., Bigot, S., Moron, V., 2000. Le domaine forestier africain et ses marges : les transitions
820   climatiques majeures à l'époque actuelle et au cours des derniers millénaires. In Servant, M., Servant-
821   Vildary, S. (eds). Dynamique à long terme des écosystèmes forestiers intertropicaux, chapter 25,
822   UNESCO.

823   Maley, J., Giresse, P., Doumenge, C., Favier, C., 2012. Comment on "Intensifying Weathering and Land Use in
824   Iron Age Central Africa." Science 337, 1040–1040. doi:10.1126/science.1221820

825   Marsset, T., Droz, L., 2010. REPREZAI_LEG1 cruise, Pourquoi Pas? R/V. doi:10.17600/10030170

826   Marsset, T., Droz, L., Dennielou, B., Pichon, E., 2009. Cycles in the architecture of the Quaternary Zaïre
827   turbidite system: a possible link with climate. Extern. Controls Deep-Water Depositional Syst. 89–106.

828   Martins, O., Probst, J.L., 1991. Biogeochemistry of major African rivers: Carbon and minerals transport, in
829   Degens, E.T., Kempe, S., Richey J.E. (eds). Biogeochemistry of Major World Rivers. SCOPE 42, 127–
830   156.

831   Métivier, F., Gaudemer, Y., 1999. Stability of output fluxes of large rivers in South and East Asia during the last
832   2 million years: Implications on floodplain processes. Basin Research 11, 293–303, doi:10.1046/j.1365-
833   2117.1999.00101.x

834   Matmon, A., Bierman, P.R., Larsen, M.C., Southworth, S., Pavich, M., Caffee, M., 2003. Temporally and
835   spatially uniform rates of erosion in the southern Appalachian Great Smoky Mountains. Geology 31,
836   155–158.

837   Meybeck, M., 2003. Global analysis of river systems: from Earth system controls to Anthropocene controls. Phil.
838   Trans. R. Soc. B 358, 1935–1955.

839   Michalopoulos, P., Aller, R.C., 2004. Early diagenesis of biogenic silica in the Amazon delta : Alteration,
840   authigenic clay formation, and storage. Geochimica and Cosmochimica Acta 68, 1061-1085.

841   Morehead, M.D., Syvitski, J., Hutton, E.W.H., Peckham, S.D., 2003. Modeling the temporal variability in the
842   flux of sediment from ungauged river basins. Global and Planetary Change 39, 95-110.

843   Morin-Rivat, J., Fayolle, A., Gillet, J.-F., Bourland, N., Gourlet-Fleury, S., Oslisly, R., Bremond, L., Bentaleb,
844   I., Beeckman, H., Doucet, J.-L., 2014. New evidence of human activities during the Holocene in the
845   lowland forests of the northern Congo basin. Radiocarbon 56(1), 209-220.

846   Neumann, J., 1955. Latitudinal variation of tropospheric temperature lapse rate. Archiv für Meteorologie,
847   Geophysik und Bioklimatologie, Serie A 8(4), 351-353.

848   Neumann, K., Eggert, M.K.H., Oslisly, R., Clist, B., Denham, T., Maret, P. de, Ozainne, S., Hildebrand, E.,
849   Bostoen, K., Salzmann, U., Schwartz, D., Eichhorn, B., Tchiengué, B., Höhn, A., 2012. Comment on
850   "Intensifying Weathering and Land Use in Iron Age Central Africa." Science 337, 1040–1040.
851   doi:10.1126/science.1221747

852   Nkounkou, R.R., Probst, J.L., 1987. Hydrology and geochemistry of the Congo River system. In Degens E.T. et
853   al. (eds). Transport of Carbon and Minerals in Major World Rivers, Part 4. Mitt. Geol-Paläont. Insti.
854   Univ. Hambourg, SCOPE/UNEP Sond. 64, 483-508.

855   O'Loughlin, F., Trigg, M.A., Schumann, G.J.P., Bates, P.D., 2013. Hydraulic characterization of the middle
856   reach of the Congo River, Water Resource Research 49, 5059–5070, doi:10.1002/wrcr.20398.

857   Osmaston, H.A., Harrison, S.P., 2005. Quaternary glaciations of Africa: A regional synthesis. Quaternary
858   International 138-139, 32-54.

859   Peckham, S.D., 2009. Geomorphometry in RiverTools, In: Hengl, T., Reuter, H.I. (eds), Geomorphometry:
860   Concepts, Software and Applications, Chapter 18, Developments in Soil Science 33, 411-430.

861   Pelletier, J.D., 2012. A spatially distributed model for the long-term suspended sediment discharge and delivery
862   ratio of drainage basins. Journal of Geophysical Research 117, F02028, doi:10.1029/2011JF002129

863   Phillips, J.D., 2003. Alluvial storage and the long-term stability of sediment yields. Basin Research 15(2), 153–
864   163, doi: 10.1046/j.1365-2117.2003.00204.x.

865   Picot, M., 2015. Cycles sédimentaires dans le système turbiditique ud Congo : nature et origine. PhD thesis,
866   Université de Bretagne Occidentale, Brest. 368 pp.

867   Picot, M., Droz, L., Marsset, T., Dennielou, B., Bez, M., 2016. Controls on turbidite sedimentation: Insights
868   from a quantitative approach of submarine channel and lobe architecture (Late Quaternary Congo Fan).
869   Marine and Petroleum Geology 72, 423-446.

870   Picouet, C., Hingray, B., Olivry, J.C., 2001. Empirical and conceptual modelling of the suspended sediment
871   dynamics in a large tropical African river: the Upper Niger River basin. Journal of Hydrology 250, 19-39.

872   Rabouille, C., Caprais, J.-C., Lansard, B., Crassous, P., Dedieu, K., Reyss, J.-L., Khripounoff, A., 2009. In situ
873   measurements of sediment oxygen consumption and organic matter budget in the Southeast Atlantic
874   continental margin close to the Congo Canyon. Deep Sea Research Part II 56, 2223–2238.

875   Regard, V., Carretier, S., Boeglin, J.-L., Ndam Ngoupayou, J.-R., Dzana, J.-G., Bedimo Bedimo, J.-P., Riotte, J.,
876   Braun, J.-J., 2016. Denudation rates on cartonic landscapes: comparison between suspended and

877   dissolved fluxes, and 10Be analysis in the Nyong ans Sanaga River basins, south Cameroon. Earth
878   Surface Processes and Landforms 41, 1671-1683. doi: 10.1002/esp.3939

879 Reichenstein, M., Bahn, M., Ciais, P., Frank, D., Mahecha, M.D., Seneviratne, S.I., Zscheischler, J., Beer, C.,
880   Buchmann, N., Frank, D.C., Papale, D., Rammig, A., Smith, P., Thonicke, K., van der Velde, M., Vicca,
881   S., Walz, A., Wattenbach, M., 2013. Climate extremes and the carbon cycle. Nature 500, 287-295.

882 Rodier, J., 1964. Régimes hydrologiques de l'Afrique Noire à l'Ouest du Congo. Mem. ORSTOM 6, 137 pp.

883 Rogers, R.D., Schumm S.A., 1991. The effect of sparse vegetative cover on erosion and sediment yield, J.
884   Hydrol. 123, 19 – 24. doi:10.1016/0022-1694(91)90065-P.

885 Roller, S., Wittmann, H., Kastowski, M., Hinderer, M., 2012. Erosion of the Rwenzori Mountains, East
886   African Rift, from in situ-produced cosmogenic 10Be. Journal of Geophysical Research 117, F03003. DO
887   I: 10.1029/2011JF002117

888 Rommerskirchen, F., Eglinton, G., Dupont, L., Rullkötter, J., 2006. Glacial/interglacial changes in southern
889   Africa: Compound-specific d13C land plant biomarker and pollen records from southeast Atlantic
890   continental margin sediments. Geochem. Geophys. Geosyst. 7, Q08010. doi:10.1029/2005GC001223.

891 Savoye, B., 1998. ZAIANGO1 cruise, L'Atalante R/V. doi:10.17600/98010100

892 Savoye, B., Babonneau, N., Dennielou, B., Bez, M., 2009. Geological overview of the Angola–Congo margin,
893   the Congo deep-sea fan and its submarine valleys. Deep Sea Res. Part II Top. Stud. Oceanogr. 56, 2169–
894   2182. doi:10.1016/j.dsr2.2009.04.001

895 Schneider, R.R., Price, B., Müller, P.J., Kroon, D., Alexander, I., 1997. Monsoon related variations in Zaire
896   (Congo) sediment load and influence of fluvial silicate supply on marine productivity in the east
897   equatorial   Atlantic   during   the   last   200,000   years.   Paleoceanography   12,   463–481.
898   doi:10.1029/96PA03640

899 Sichingabula, H.M., (1999). Special study on sediment discharge and its consequence: analysis and results of
900   discharge and sediment monitoring activities in the southern Lake Tanganyika basin, Zambia. Technical
901   report number 4. UNDP/GEF. Dar es Salaam, Tanzania, 106 pp.

902 Simpson, G., Castelltort, S., 2012. Model shows that rivers transmit high-frequency climate cycles to the
903   sedimentary record. Geology 40(12), 1131-1134. doi:10.1130/G33451.1

904 Sionneau, T., Droz, L., Marsset, T., Dennielou, B., Bez, M., 2010. Congo-Zaire detrital supply variability during
905   the last 200 ka: a possible explanation for the longitudinal migration of the Zaire fan depocenters. 18th
906   International Sedimentological Congress, 26/09 to 01/10 2010, Mendoza (Argentine).

907 Spencer, R.G.M., Hernes, P.J., Dinga, B., Wabakanghanzi, J.N., Drake, T.W., Six, J., 2016. Origins, seasonality,
908   and   fluxes   of   organic   matter   in   the   Congo   River,   Global   Biogeochem.   Cycles   30,
909   doi:10.1002/2016GB005427.

910 Summerfield, M.A., Hulton, N.J., 1994. Natural controls of fluvial denudation rates in major world drainage
911   basins. J. Geophys. Res. Solid Earth 99, 13871–13883. doi:10.1029/94JB00715

912 Syvitski, J.P.M., Morehead, M.D., Nicholson, M., 1998. Hydrotrend: a climate-driven hydrologic-transport
913   model for predicting discharge and sediment load to lakes or oceans. Computers & Geosciences 24, 51-
914   68.

915 Syvitski, J.P.M., Morehead, M.D., 1999. Estimating river-sediment discharge to the ocean: application to the Eel
916   margin, North California. Marine Geology 154,13–28.

917 Syvitski, J.P.M., Milliman, J., 2007. Geology, geography, and humans battle for dominance over the delivery of
918   fluvial sediment to the coastal ocean. The Journal of Geology 115, 1–19.

919 Syvitski, J.P.M., Morehead, M.D., Bahr, D.B., Mulder, T., 2000. Estimating fluvial sediment transport: The
920   rating parameters. Water Resources Research 36(9), 2747-2760.

921 Syvitski, J.P.M., Morehead, M.D., Nicholson, M., 1998. HydroTrend: a climate-driven hydrologic-transport
922   model for predicting discharge and sediment load to lakes or the ocean. Comput Geosci 24(1), 51–68.

923 Syvitski, J.P.M., Vörösmarty, C.J., Kettner, A.J., Green, P., 2005. Impact of humans on the flux of terrestrial
924   sediment to the global coastal ocean. Science 308, 376-380.

925 Syvitski, J.P.M., Kettner, A.J., Overeem, I., and Brakenridge, G.R., 2017. Latitudinal controls on siliciclastic
926   sediment   production   and   transport.   SEPM   Special   Publication   No.   108.   Doi:
927   http://dx.doi.org/10.2110/sepmsp.108.04.

928 Thiry, M., 2000. Paleoclimatic interpretation of clay minerals in marine deposits: an outlook from the continental
929   origin. Earth Science Review 49, 201–221.

930   Tucker, C.J., 1979. Red and Photographic Infrared Linear Combinations for Monitoring Vegetation, Remote
931   Sensing of Environment 8(2),127-150.

932   Vance, D., Bickle, M., Ivy-Ochs, S., Kubik, P.W., 2003. Erosion and exhumation in the Himalaya from
933   cosmogenic isotope inventories of river sediments. Earth and Planetary Science Letters 206, 273–288.

934   Vangriesheim, A., Pierre, C., Aminot, A., Metzl, N., Baurand, F., Caprais, J.C., 2009. The influence of Congo
935   River discharges in the surface and deep layers of the Gulf of Guinea, Deep Sea Research Part II 56,
936   2183–2196.

937   Vanmaercke, M., Poesen, J., Broeckx, J., Nyssen, J., 2014. Sediment Yield in Africa. Earth-Science Reviews
938   136, 350-368. doi: 10.1016/j.earscirev.2014.06.004

939   Vörösmarty C.J., Meybeck, M., Fekete, B., Sharma, K., 1997. The potential impact of neo-Castorization on
940   sediment transport by the global network of rivers. In: Walling D., Probst, J.L. eds., Human Impact of
941   erosion and sedimentation. IAHS Press, Wallingford, UK., 261–272.

942   Walling, D.E., 2006. Human impact on land–ocean sediment transfer by the world's rivers. Geomorphology 79,
943   192–216.

944   Wang, J.-J., Adler, R.F., Huffman, G.J., Bolvin, D., 2014. An updated TRMM composite climatology of tropical
945   rainfall and its validation. J. Climate 27, 273-284.

946   Weijers, J.W.H., Schefuss, E., Schouten, S., Sinninghe Damsté J.S., 2007. Coupled Thermal and Hydrological
947   Evolution of Tropical Africa over the Last Deglaciation. Science 315, 1701-1704. doi:
948   10.1126/science.1138131.

949   Weldeab, S., Lea, D.W., Schneider, R.R., Andersen. N., 2007. 155,000 Years of West African Monsoon and
950   Ocean Thermal Evolution. Science 316, 1303-1307. doi: 10.1126/science.1140461

951   Wilby, R.L., Dalgleish, H.Y., Foster, I.D.L., 1997. The impact of weather patterns on historic and contemporary
952   catchment sediment yields. Earth Surface Processes and Landforms 22, 353–63.

953   Winemiller, K.O. et al., 2016. Balancing hydropower and biodiversity in the Amazon, Congo and Mekong.
954   Science 351, 128–129.

955   Wittmann, H., von Blanckenburg, F., Maurice, L., Guyot, J.-L., Filizola, N., Kubik, P.W., 2011. Sediment
956   production and delivery in the Amazon River basin quantified by in situ-produced cosmogenic nuclides
957   and recent river loads. GSA bulletin 123(5-6), 934-950. doi: 10.1130/B30317.1

958   Wotzka, H.P., 2006. Records of activity: radiocarbon and the structure of Iron Age settlement in Central Africa.
959   In: Wotzka, H.P., ed. Grundlegungen. Beiträgezur europäischen und afrikanischen Archäologie für
960   Manfred K.H. Eggert. Tübingen: Francke Attempto Verlag, 271–289.

961   Xie, Y., Sha, Z., Yu, M., 2008. Remote sensing imagery in vegetation mapping: a review. Journal of Plant
962   Ecology 1(1), 9-23.

963   Xu, J.X., 2003. Sediment flux to the sea as influenced by changing human activities and precipitation: example
964   of the Yellow River, China. Journal of Environmental Management 31(3), 328–41.

965   Zomer, R.J., Trabucco, A., Bossio, D.A., Verchot, L.V., 2008. Climate change mitigation: A spatial analysis of
966   global land suitability for clean development mechanism afforestation and reforestation. Agriculture
967   Ecosystems and Environment 126, 67-80.

968   Zhang, Q., Justice, C.O., Jiang, M., Brunner, J., Wilkie, D.S., 2006. A GIS-based assessment on the vulnerability
969   and future extent of the tropical forests of the Congo basin. Environmental Monitoring and Assessment
970   114, 107-121.

971   Zhu, Y.M., Lu, X.X., Zhou, Y., 2007. Suspended sediment flux modeling with artificial neural network: an
972   example of the Longchuanjiang River in the upper Yangtze catchment, China. Geomorphology 84,111–
973   125.

974

Figures

976
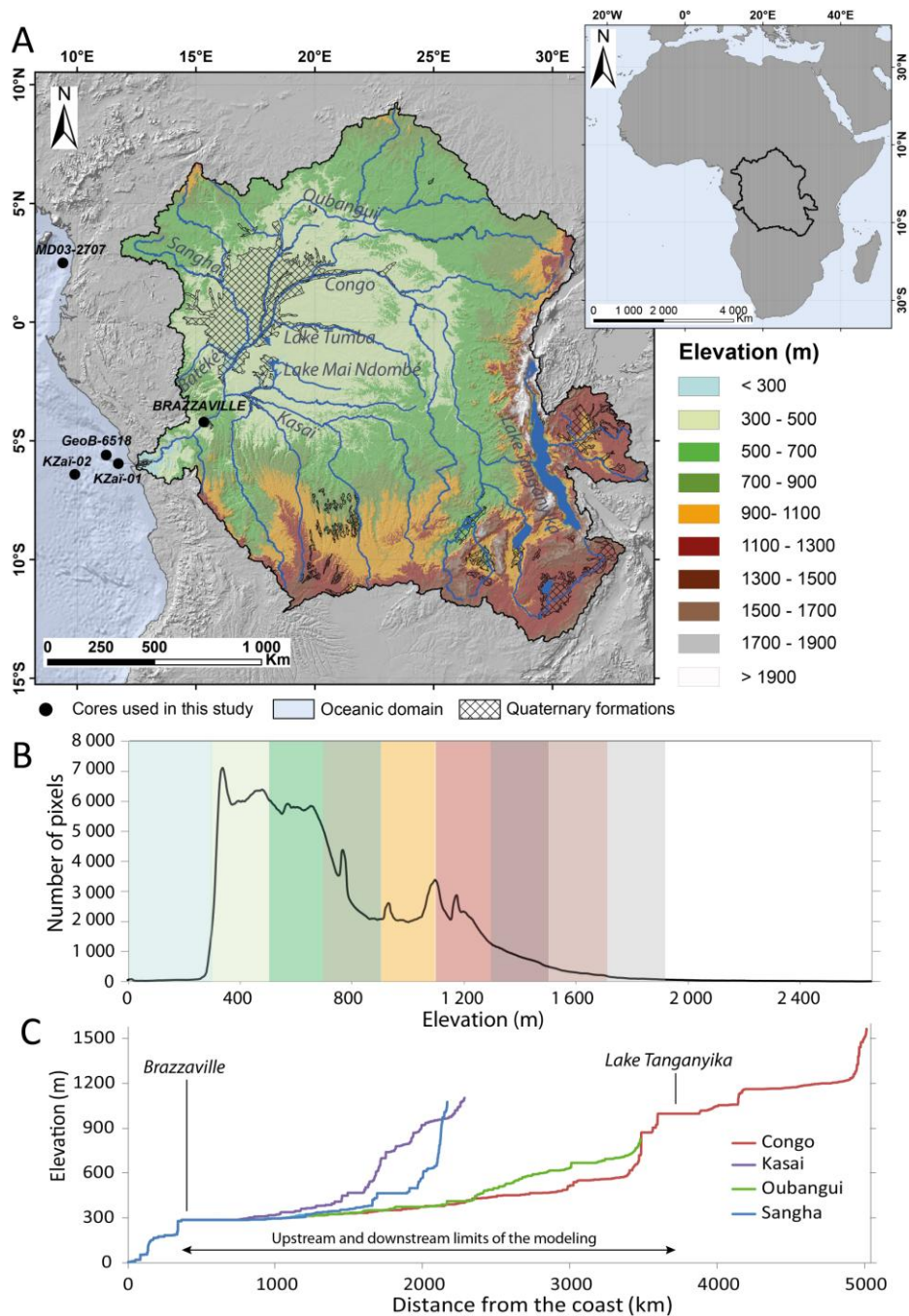
Figure 1: Geomorphological setting of the Congo catchment. A) Drainage basin represented by elevation, where dark blue indicates the Congo River with its major tributaries and lakes, location of datasets used and Quaternary deposits. B) Statistical distribution of elevation within the catchment. C) Longitudinal profiles of the Congo River and its main tributaries, with upstream and downstream boundaries of the modeling. Note that the knickpoint on the Congo River profile at Brazzaville indicates that regressive erosion due to the successive marine oscillations in Quaternary does not affect the morphology of the catchment above this point.
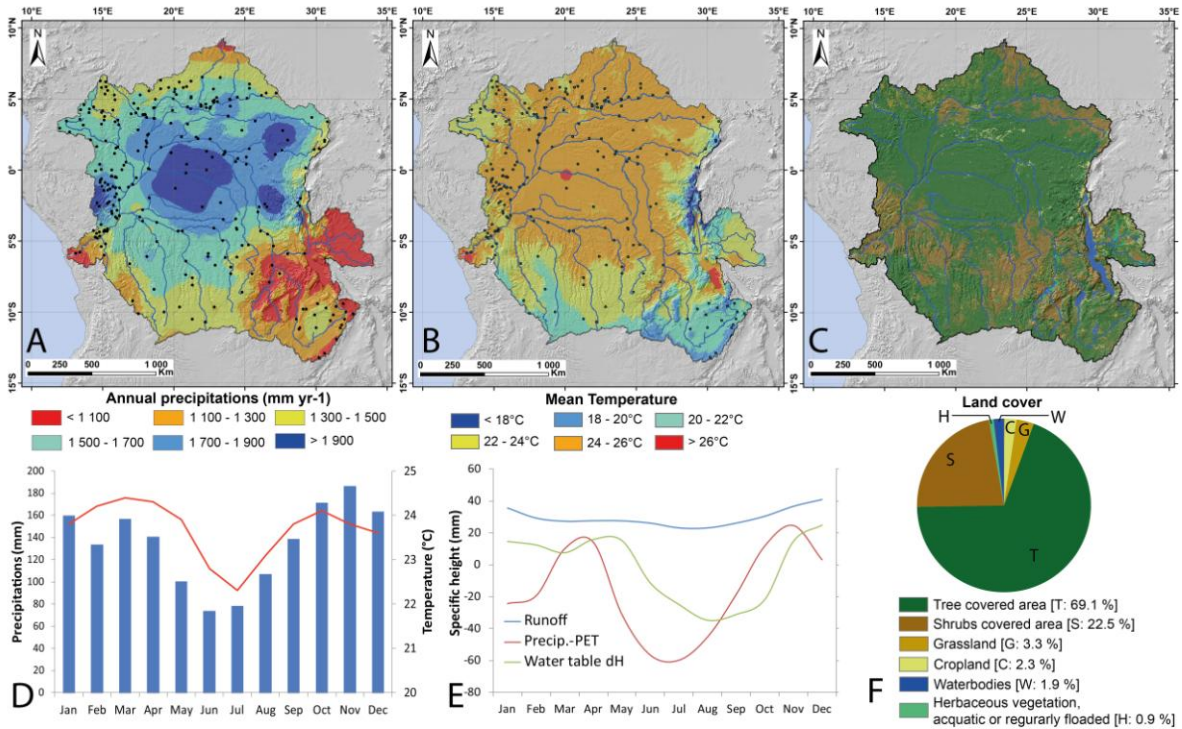
Figure 2: Environmental setting of the Congo catchment. A) Spatial distribution of annual precipitations (data from Hijmans et al., 2005) and location of the SIEREM stations used for calculation of temporal precipitation standard variation. B) Spatial distribution of mean annual temperature (data from Hijmans et al., 2005). C) Spatial distribution of land cover (data from Latham et al., 2014). D) Mean monthly precipitations (blue bars) and temperature (red line). E) Monthly water balance, with runoff (blue) (data from Laraque et al., 2013), available water (precipitation minus potential evapo-transpiration (PET; Zomer et al., 2008, in red) and variations in water table height (from lakes-level satellite-monitoring; Crétaux et al., 2011; Becker et al., 2014, in green). F) Quantitative repartition of land cover.
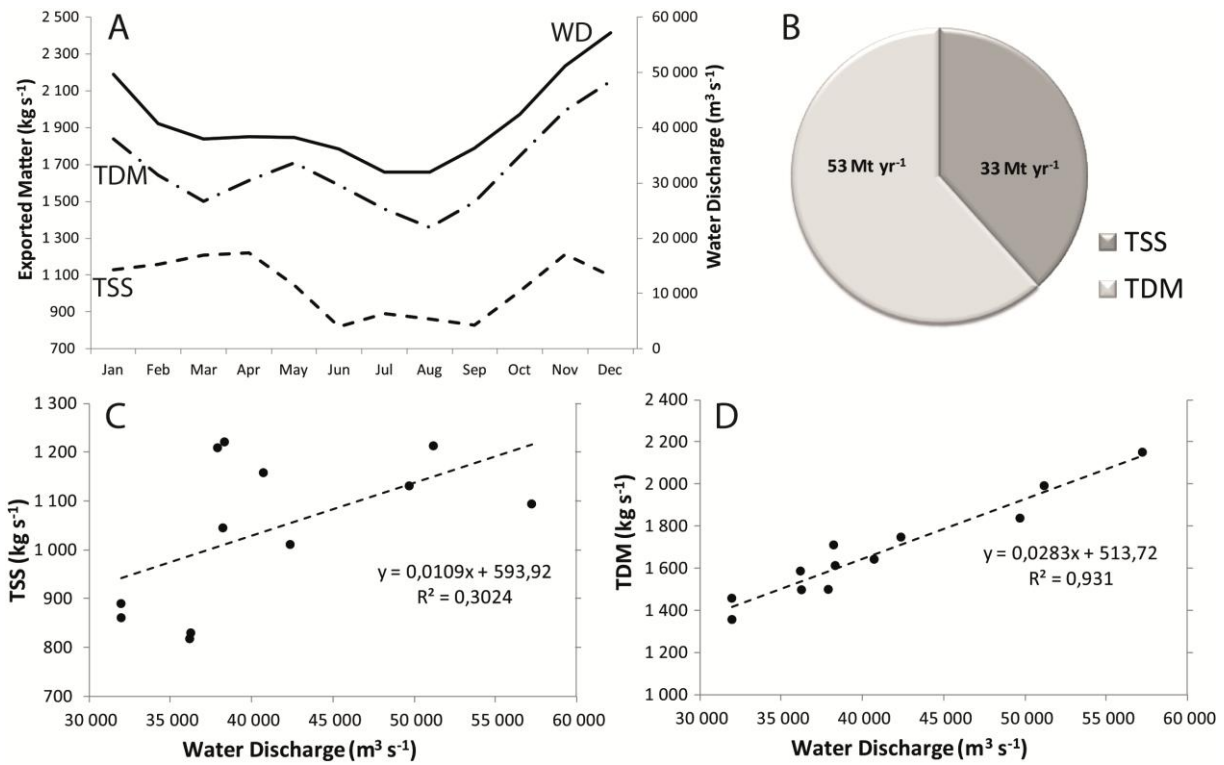
Figure 3: Mean monthly water and sediment discharge of the Congo watershed, in-situ monitored at Brazzaville gauging station (from Laraque et al., 2013). A) Monthly water discharge (WD; solid line), monthly Total Suspended Sediments (TSS; regular-dashed line), monthly Total Dissolved Matter (TDM, dashed line with dots). B) Annual sediment yield (Total Suspended Sediments and Total Dissolved Matter, respectively) exported from the Congo catchment. C) Relation between mean monthly TSS and mean monthly water discharge. D) Relation between mean monthly TDM and mean monthly water discharge.
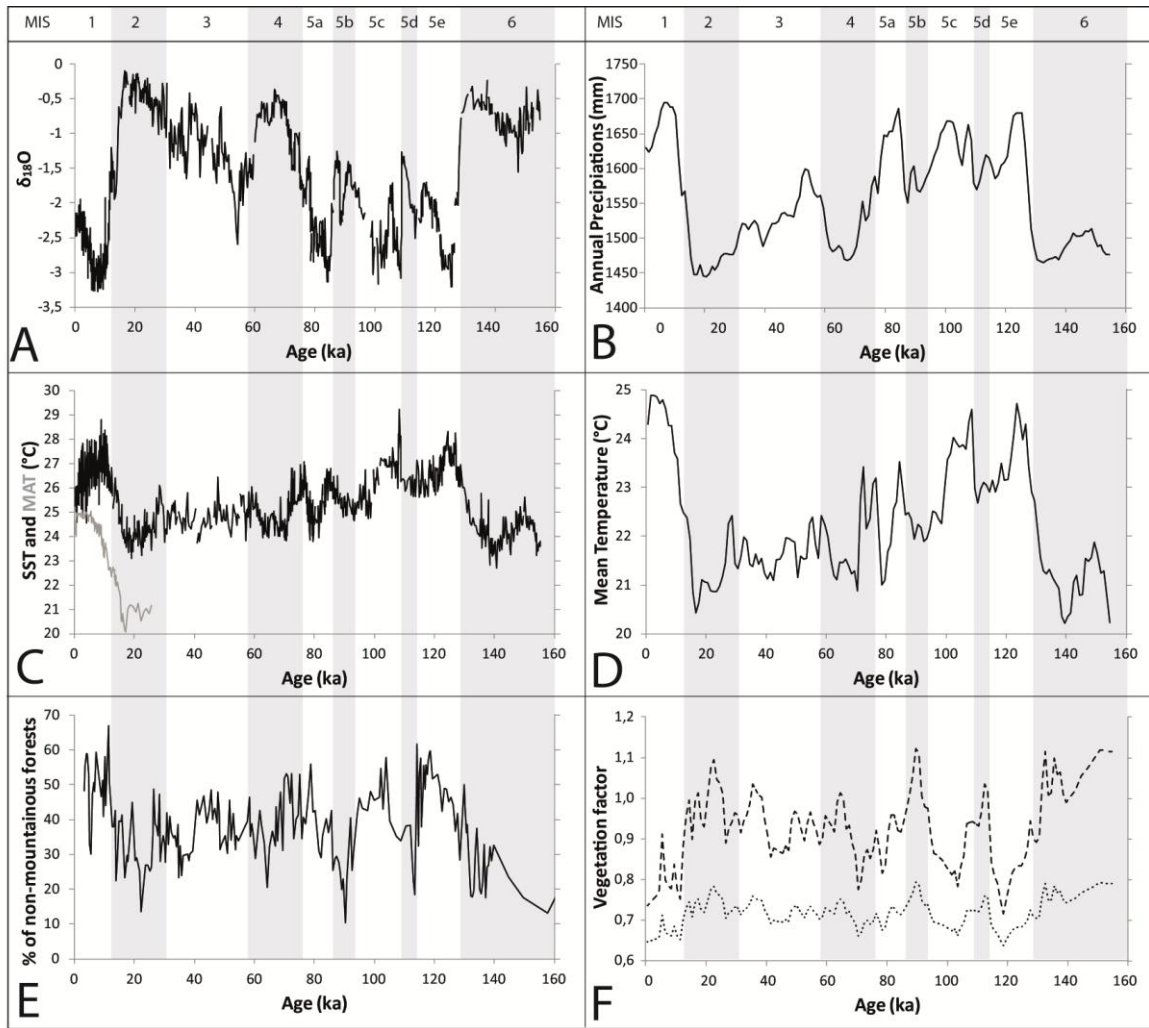
1004

1005 Figure 4: Evolution of different marine proxies over the last 155 ka (A, C, E), used for the
1006 interpretation of environmental changes (B, D, F). A) $\delta^{18}O$ curve of the MD03-2707 core which is
1007 located in the Guinea Gulf (Weldeab et al., 2007). B) Interpretation of $\delta^{18}O$ data in terms of
1008 precipitation changes, since these data are interpreted as representative of the monsoon intensity
1009 (Weldeab et al., 2007; Caley et al., 2011). C) Sea Surface Temperature curve (SST, black line) of the
1010 MD03-2707 core (Weldeab et al., 2007) and Mean Atmospheric Temperature (MAT, grey line) of the
1011 GeoB6518-1 core (Weijers et al., 2007). D) Interpretation of SST and MAT in terms of mean
1012 catchment temperatures. For B and D, the calibration is performed to present-day (Hijmans et al.,
1013 2005) and the LGM (Gent et al., 2011) from global climatic model CCSM4 values and the data are
1014 smoothed by applying a mean value for: i) a 1 ka step for the 155 ka simulation, and ii) a 200 years
1015 step for the 23 ka simulation. E) Percentage of non-mountainous forests pollens for the KZaï-02 core
1016 (Dalibard et al., 2014). F) Interpretation of non-mountainous forests pollens in terms of vegetation
1017 factor (method detailed in text). The dotted line represents the minimum value and the dashed line the
1018 maximum.

1019
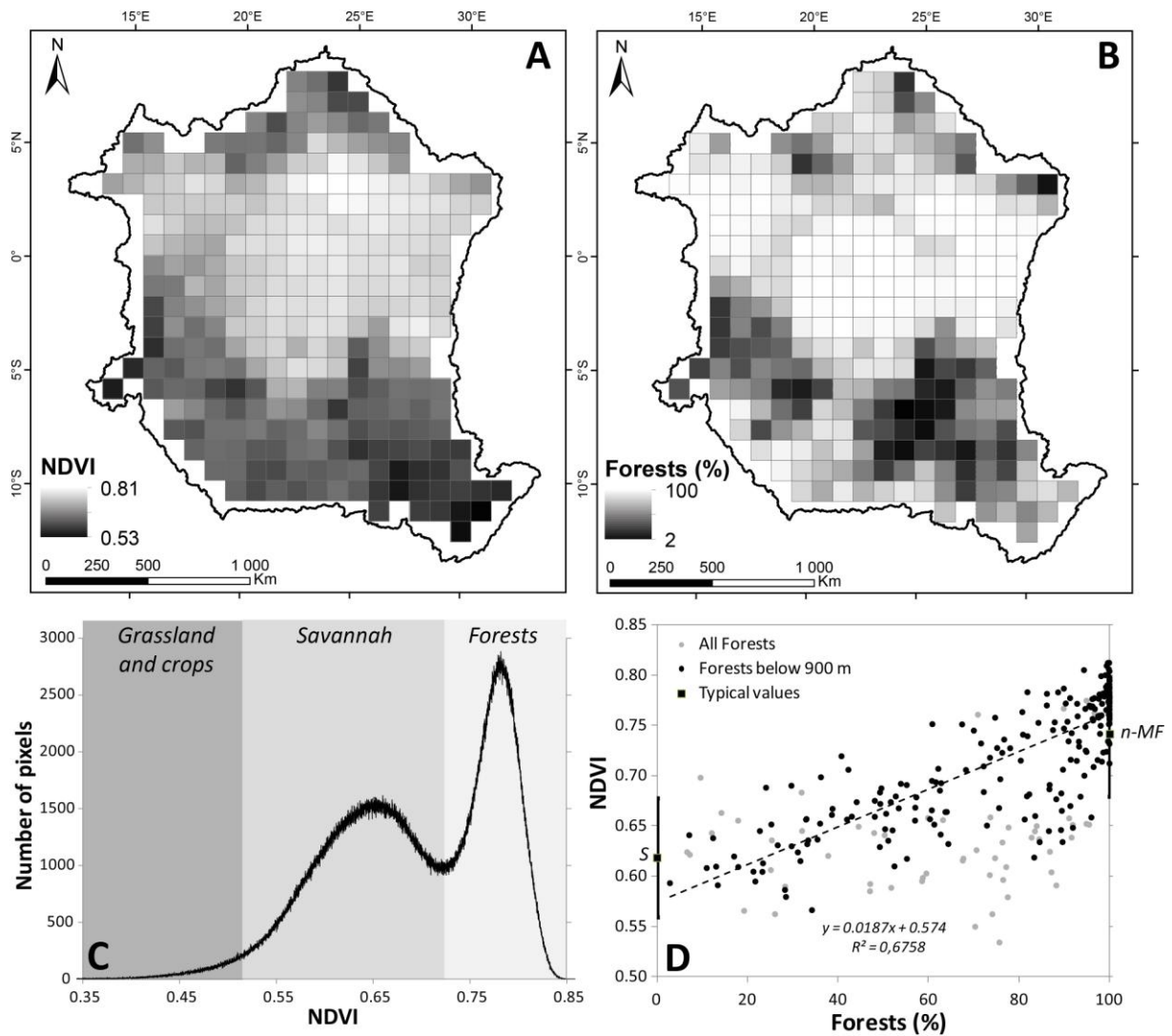
Figure 5: The relation between NDVI (Normalized Difference Vegetation Index) and spatial Forest distribution. A) Mean annual NDVI averaged for 100 x 100 km tiles. B) Mean percentage of forests averaged for 100 x100 km tiles. C) Statistical distribution of NDVI and type of land cover associated. D) Correlation between mean NDVI and mean percentage forest, averaged for 100 x 100 km tiles. The vertical black bars at 0 and 100 % correspond to the range of NDVI values for savannah (S) and non-mountainous forests (n-MF). Equation and R² are given only for non-mountainous forests (black dots).
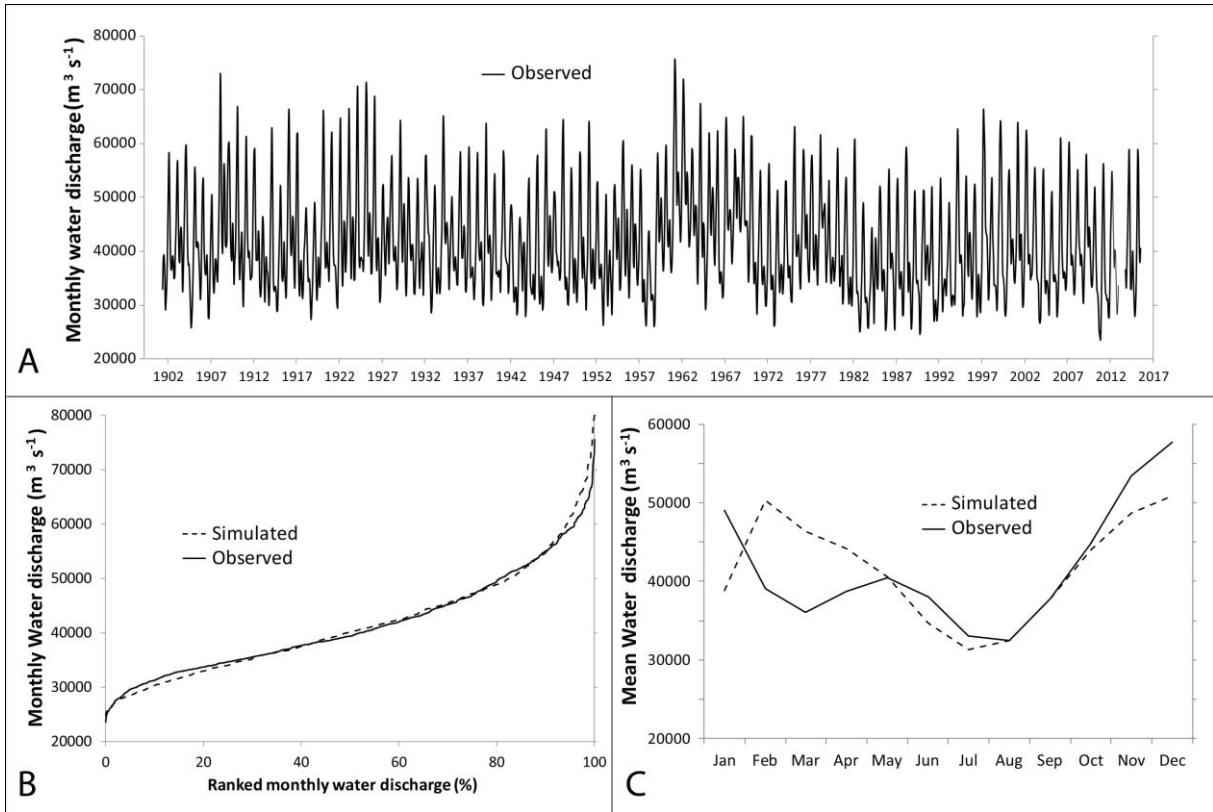
Figure 6: Calibration of simulated water discharge with present-day data. A) Observed, 114 years of monthly discharge data at the Brazzaville gauging station (Laraque et al., 2013a; HYBAM, 2016). B) Ranked monthly observed (solid line) and simulated (dashed line) water discharge. C) Monthly observed and simulated mean water discharge. These data highlight the capability of the HydroTrend model to simulate realistic discharges for the Congo River at Brazzaville.

31
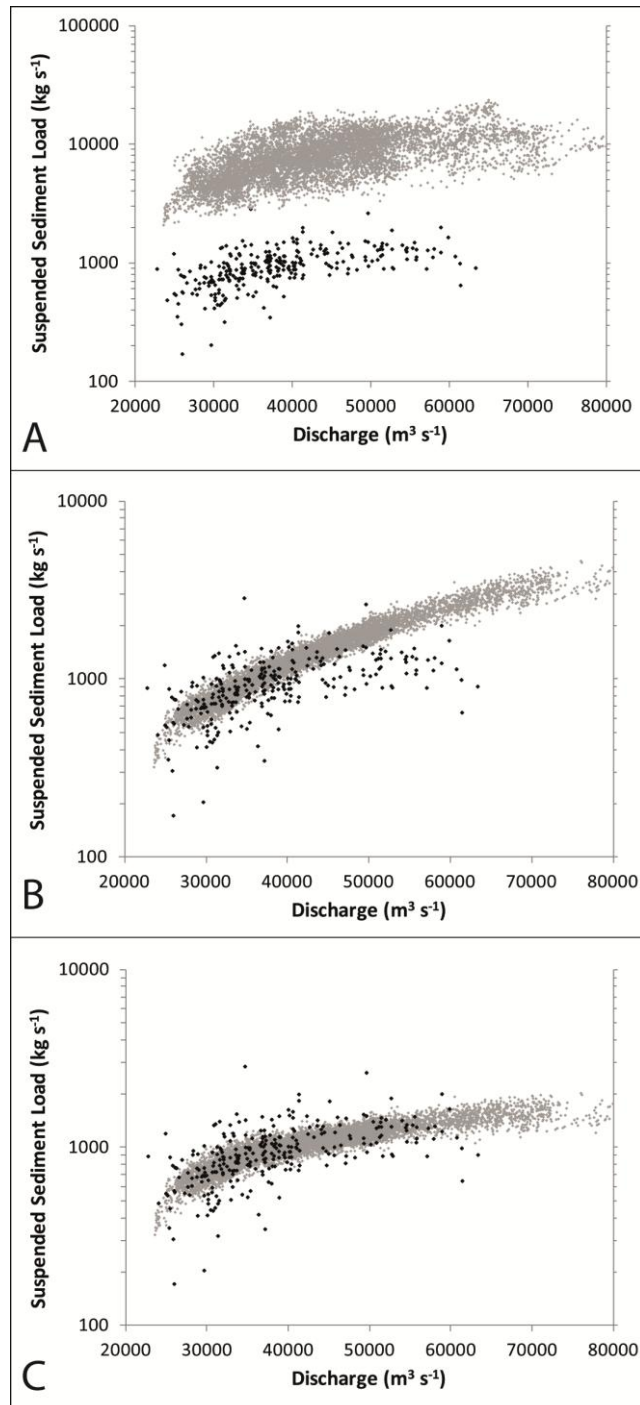
1035

Figure 7: Calibration of simulated suspended sediment load with present-day observed data. The graphs A, B and C show the relation between suspended sediment load and water discharge. Observed data are represented as black dots; 20 years of daily simulated data are represented as grey dots. A) Simulations without trapping. B) Simulation including classic trapping (i.e. trapping by a lake) in the Cuvette Centrale. C) Simulation including classic and floodplain trapping when discharge exceed bankfull discharge ($>33,000$ m^3 s^{-1} for the best fit). To match simulated to observed data, sediment trapping by involving at least two distinct processes is needed.

1036
1037
1038
1039
1040
1041
1042

1043
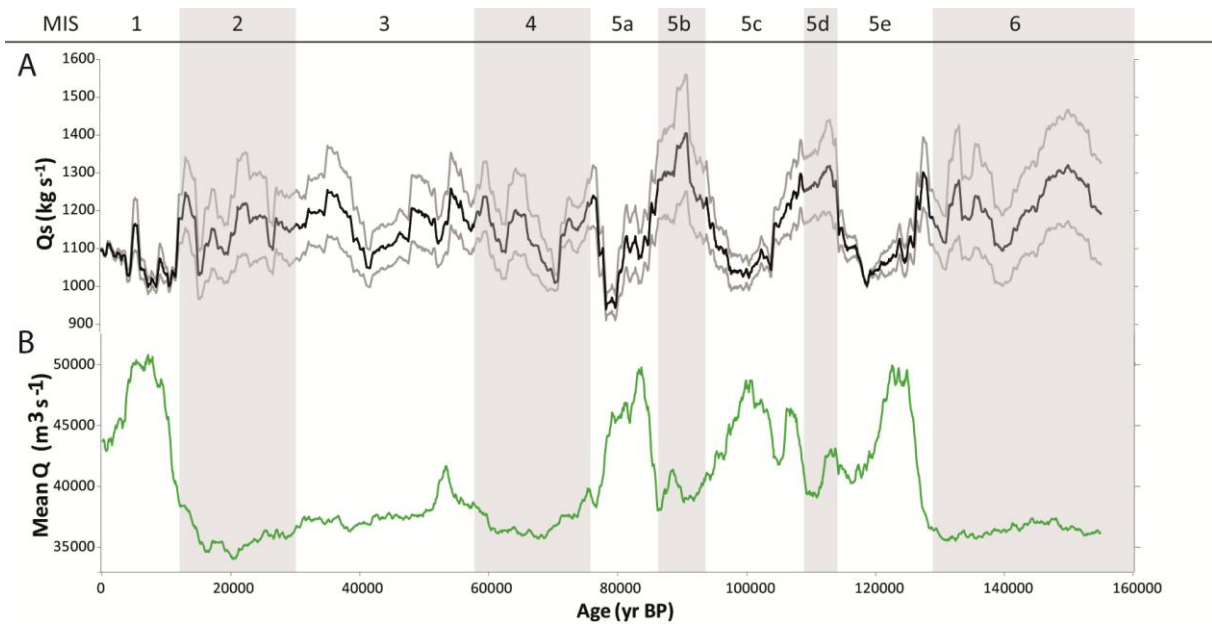
1044

1045 Figure 8: HydroTrend simulations of sediment load and water discharge over the last 155 ka. A)

1046 Simulated suspended sediment load evolution (Qs). The black curve corresponds to the mean sediment

1047 load, grey curves are the minimum and maximum with respect to vegetation index. B) Simulated

1048 water discharge. Curves A and B are running averages over 500 years of mean annual data simulated.

1049
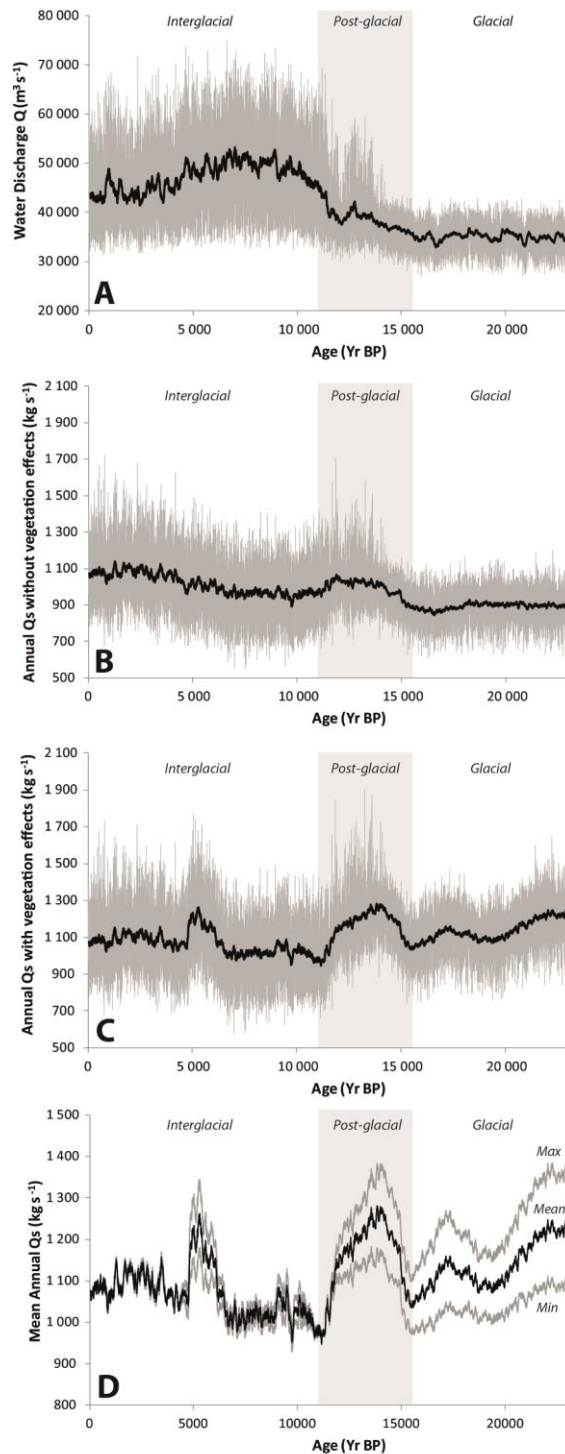
1050

Figure 9: Water and suspended sediment simulation results focused over the last 23 ka. Gray curves

represent annual data, while black curves are running means over 100 years. Three climatic periods

(interglacial, post-glacial and glacial) are individualized by the light gray/white bands in background.

A) Water discharge. B) Suspended sediment load without taking into account vegetation changes. C)

Mean suspended sediment load taking into account vegetation changes. D) Running mean over 100

years of minimum (lower grey line), maximum (upper gray line) and mean (black line) suspended
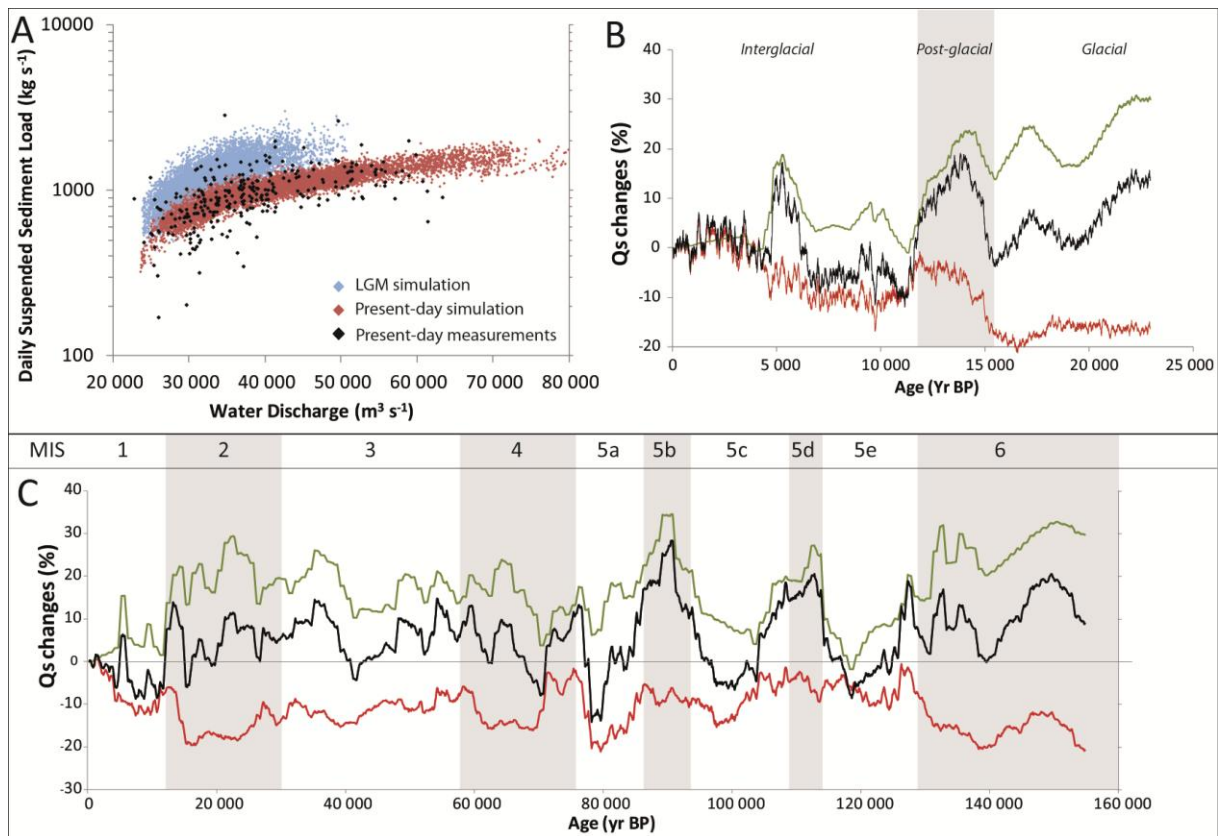
sediment load.

Figure 10: A) Relation between suspended sediment load and water discharge during present-day (observed data are represented with black triangles; 20 years of daily simulated data are represented with red triangles) and LGM conditions (20 years of daily simulation data are represented in blue). B) Deciphering the effect of only climate (without vegetation changes over time) (red curve) and only vegetation (green curve), and combined on mean suspended sediment load (black curve) for the last 23 ka. On the background, the light gray period correspond to post-glacial stage. C) Deciphering the effect of climate and vegetation over the last 155 ka. The caption is the same as B except that light gray periods correspond to cold climatic stages.

1068
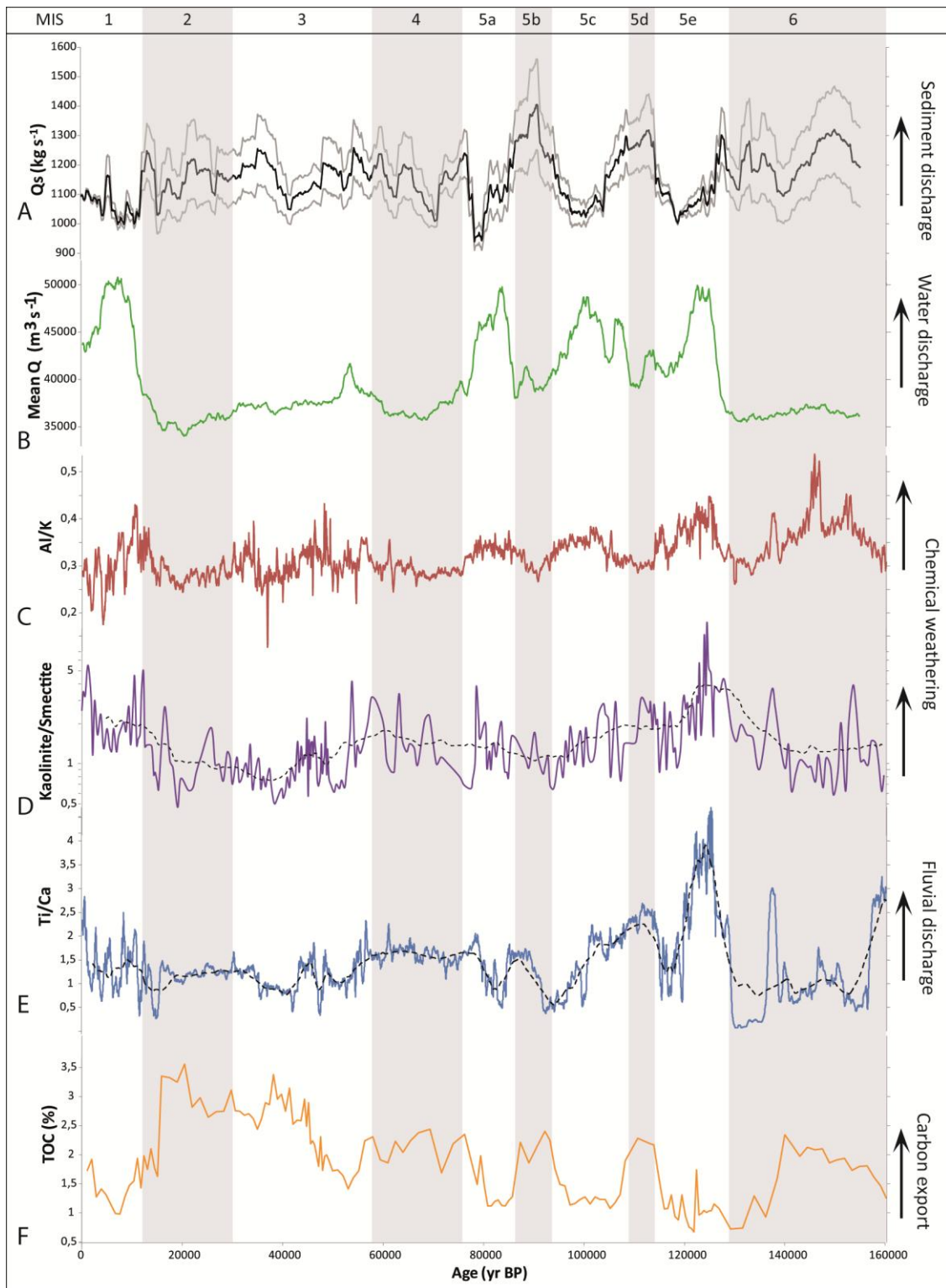
Figure 11: Comparisons of HydroTrend simulations with available offshore proxies related to sediment supply. A) and B) see caption in Fig. 8. C) Al/K semi-quantitative ratio measured with a XRF (Hatin et al., 2017). D) Log of Kaolinite/Smectite ratio (Sionneau et al., 2010). E) Ti/Ca semi-quantitative ratio measured with a XRF. F) Total Organic Carbon (TOC). Curves C to F were drawn from XRF measurements from core KZaï-02 (location in Figure 1). The dashed lines in D and E are running averages. In the background, the light gray periods correspond to cold climatic stages.

36

Table captions

1076   Table 1: Values of parameters used in simulations.

Parameters	Value	Unit	Référence
Present-day yearly temperature	24.6	°C	Alsdorf et al., 2016
Standard deviation of yearly temperature	1.44	°C	Alsdorf et al., 2016
Present-day yearly precipitation	1630.1	mm	Alsdorf et al., 2016
Standard deviation of yearly precipitation	563	mm	Alsdorf et al., 2016
Precipitation mass balance coeficient	1		Syvitski et al., 1998
Distribution exponential	1.7		Syvitski et al., 1998
Distribution range	9		Syvitski et al., 1998
Constant annual baseflow	22000	$m^3.s^{-1}$	Alsdorf et al., 2016
Monthly Temperature	see Fig. 2D	°C	Hijmans et al., 2005
Monthly Precipitation	see Fig. 2D	mm	Hijmans et al., 2005
Lapse rate	6.4	$°C.km^{-1}$	Neumann, 1955
ELA start	4500	m	Osmaston and Harrison, 2005
Dry precipitation evaporation fraction	0		Syvitski et al., 1998
Average slope of the river bed delta	0.000183625		DEM
River lenght	4700	km	DEM
Volume of reservoirs	1000	km^3	DEM and our calibration
Altitude of reservoirs	290	m	DEM
Velocity coeficient (k)	0.56		Leopold and Maddock, 1953
Velocity exponent (m)	0.1		Leopold and Maddock, 1953
Width coeficient (a)	6.62		Leopold and Maddock, 1953
Width exponent (b)	0.61		Leopold and Maddock, 1953
Average velocity	1.23	$m^3.s^{-1}$	Laraque et al., 1995
Maximum groundwater storage	6.10^11	m^3	Cretaux et al., 2011; Becker et al., 2014
Minimum groundwater storage	10^11	m^3	Cretaux et al., 2011; Becker et al., 2014
Initial groundwater storage	3.5.10^11	m^3	Cretaux et al., 2011; Becker et al., 2014
Groundwater coeficient	15000	$m^3.s^{-1}$	Cretaux et al., 2011; Becker et al., 2014
Groundwater exponent	1.4		Cretaux et al., 2011; Becker et al., 2014
Saturated hydraulic conductivity	315	$mm.day^{-1}$	Bear, 1972 and our calibration
Latitude of the outlet	15.3 N		DEM
Longitude of the outlet	4.283 W		DEM
Lithology factor (L)	1		Syvitski and Milliman, 2007
Anthropogenic factor	1		Syvitski and Milliman, 2007
Landcover factor	0.6444-0.7325		our calibration (min-max)
Bankfull discharge	33000	$m^3.s^{-1}$	our calibration
Altitude of bankfull discharge	350	m	DEM

1077

1078

1079

1080